THE SPIN STRUCTURE OF THE NUCLEON

MICHEL C. VETTERLI

TRIUMF, 4004 Wesbrook Mall, Vancouver, B.C. V6T 2A3, Canada

This paper gives a pedagogical introduction to our knowledge of the spin structure of the nucleon. In particular, polarised deep inelastic lepton scattering is presented as a tool to study how the nucleon's constituents combine to generate its spin. The importance of semi-inclusive measurements is discussed and a window on future experiments in the field is given.

1 Introduction

This paper gives an overview of the spin structure of the nucleon with emphasis on a pedagogical presentation of the tools used to study this fundamental property of protons and neutrons. While many of the data currently available are shown, this paper is not intended to be an exhaustive summary of the field. Rather, the data are used to illustrate the concepts presented. The most recent progress in the field can be found in the proceedings of the annual conference on deep inelastic scattering and QCD [1,2].

The last ten years have seen a wealth of measurements of the polarisation asymmetry in the cross-section for deep inelastic lepton scattering (DIS). This has been made possible by impressive advances in polarised target and beam technologies. Precise data now exist on *inclusive* polarised DIS from experiments at SLAC, CERN, and DESY. These data can be interpreted as showing that surprisingly, only about 30% of the nucleon's spin comes from the spins of the quarks. To make further progress on this problem, *semi-inclusive* measurements are needed where hadrons in coincidence with the scattered lepton are detected. These data allow us to determine the flavour of the quark that was struck and isolate the contribution to the nucleon's spin by valence and sea quarks. Furthermore, semi-inclusive data on charm production should give information on the contribution of gluons to the nucleon's spin. Current and future experiments are concentrating on semi-inclusive measurements.

After a short discussion of magnetic moments, the formalism of polarised deep inelastic scattering is presented in Sec. 3.1-3.2. The data on the polarised structure function $g_1(x)$ are then shown in Sec. 3.3 which is followed by the interpretation of these data in terms of sum rules in Sec. 4. Section 5 shows how spin dependent structure functions can be used to determine the contribution of the quark spins to the spin of the nucleon. The Q^2 evolution of $g_1(x)$ is discussed in Sec. 6, while other spin structure functions are presented in

Sec. 7. A description of the experiments which have addressed the nucleon spin problem over the last decade is given in Sec. 8. Semi-inclusive measurements, which are the current focus of the field are discussed in section 9. Finally, the future directions of the field are discussed in section 10.

2 The Spin of Three-Body States

As a preamble to the discussion on polarised deep inelastic scattering, two simple examples of how three spin $1/2$ particles combine to form a spin $1/2$ system are presented: the ground-state of ^{3}He and ^{3}H, and baryon magnetic moments.

2.1 The Nuclear 3-Body Ground State

The wave functions of ^{3}He and ^{3}H are among the most studied topics in physics. ^{3}He is made up of two protons and one neutron, each of which has a spin of $1/2$. ^{3}H has one proton and two neutrons. The total wavefunction also has a spin of $1/2$ leading to the following possibilities for the combination of the three nucleons:

$$
\begin{array}{lcl}
\text{L=0, S= 1/2} & \Rightarrow & \text{S-State } (>90\%) \\
\text{L=1, S= 1/2, 3/2} & \Rightarrow & \text{P-State } (<1\%) \\
\text{L=2, S= 3/2} & \Rightarrow & \text{D-State } (8\text{-}9\%).
\end{array}
$$

L is the orbital angular momentum of the 3-body system, while S is the total spin. Since the ground-state is overwhelmingly L=0, the two protons are anti-aligned due to the Pauli exclusion principle, and any spin effects observed in ^{3}He should come from the unpaired neutron. For example, consider the magnetic moment given by:

$$
\vec{\mu_s} = g_s \cdot \vec{s} \ ; \quad
\begin{array}{l}
g_s(\text{p}) = 5.5855, \\
g_s(\text{n}) = -3.8327.
\end{array}
$$

We would have $\mu_{\text{s}}(^3\text{He}) = \mu_{\text{s}}(\text{n})$ and $\mu_{\text{s}}(^3\text{H}) = \mu_{\text{s}}(\text{p})$ if the wave functions were purely S-state. This is approximately true in reality:

$$
\begin{array}{lcl}
\mu_{\text{s}}(^3\text{He}) = -2.2174 & \approx & \mu_s(\text{n}) = -1.9130 \\
\mu_{\text{s}}(^3\text{H}) = 2.9788 & \approx & \mu_s(\text{p}) = 2.7927.
\end{array}
$$

A large part of the difference can be ascribed to meson exchange currents. Since these have opposite sign in the two nuclei, they should cancel in the average of the magnetic moments:

$$
\begin{array}{l}
\frac{1}{2}[\mu_{\text{s}}(^3\text{H}) + \mu_{\text{s}}(^3\text{He})] = 0.4257 \\
\frac{1}{2}[\mu_{\text{s}}(\text{p}) + \mu_{\text{s}}(\text{n})] = 0.4399.
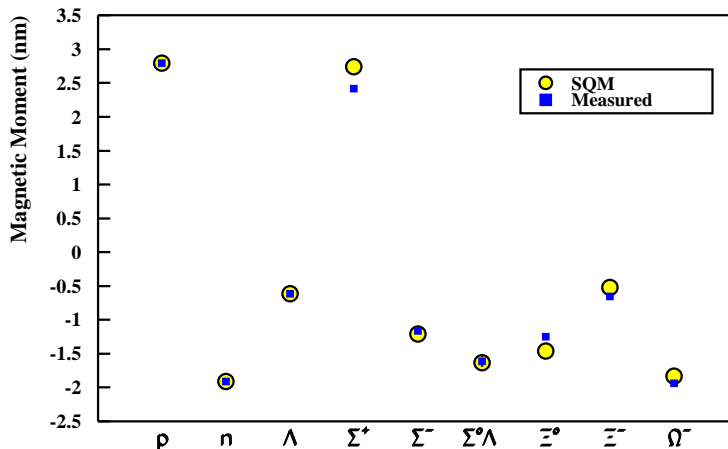\end{array}
$$

Figure 1: Baryon magnetic moments. The proton, neutron, and Λ are used as input parameters, while the other magnetic moments are predictions. The agreement of the data with the simple quark model (SQM) is very good.

The remaining difference ($\approx 3.2\%$) is due to the other components of the ground-state wavefunction (P- and D-states).

As an experimental aside, the fact that polarised ^{3}He looks very much like a polarised neutron (at least as far as spin effects are concerned) makes it an ideal polarised neutron target. This has been exploited both at SLAC (E142/E154) and at DESY (HERMES).

2.2 Baryon Magnetic Moments

Since the simple model of three spin 1/2 particles combining to form a spin 1/2 state works so well in the nuclear case, it is natural to apply it to the nucleon. However, in this case we do not know the magnetic moments of the constituents, the quarks, since they cannot be isolated. Nevertheless, we can test the simple model by looking at the ratio of $\mu_s(\mathrm{p})$ and $\mu_s(\mathrm{n})$ where the quark magnetic moments cancel. Experimentally, $\mu_s(\mathrm{p})/\mu_s(\mathrm{n}) = -1.46$, while the simple quark parton model predicts –1.50. Furthermore, we can use the proton, the neutron, and the Λ to set the values of $\mu_s(\mathrm{u})$, $\mu_s(\mathrm{d})$, $\mu_s(\mathrm{s})$, and predict the magnetic moments of the other baryons. The results are shown in Fig. 1. The agreement between the predictions and the measurements is
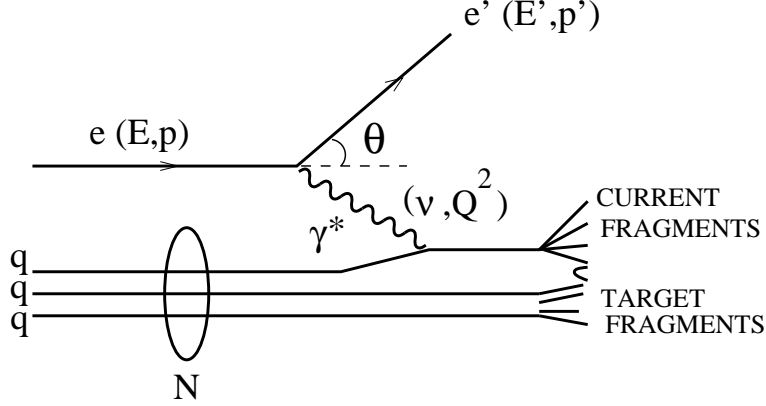
Figure 2: Diagram of the Deep Inelastic Scattering process. The incoming lepton emits a virtual photon which is absorbed by one of the quarks in the nucleon.

very good indicating that the simple model works well. However, while the magnetic moments are consistent with the model presented here, they depend only on the static properties of the nucleon wavefunction (more precisely at $Q^2 = 0$) and the rest of this paper will discuss how this picture is too simple.

3 Inclusive Polarised Deep Inelastic Scattering

3.1 Polarised DIS Formalism

The main process we will be concerned with in these lectures, deep inelastic scattering, is depicted in Fig. 2. An incoming lepton (shown here as a positron or an electron) emits a virtual photon which is absorbed by a quark in the nucleon. The nucleon is broken up and the struck quark and the target remnant fragment into hadrons in the final state. Only the lepton is detected in inclusive measurements while detection of one or more hadrons in the final state (semi-inclusive data) adds important information on the scattering process. $W^{\pm}$ and Z^0 exchanges are not important at the energies of the current spin experiments. The kinematic variables relevant for this process are listed in Table 1. The formalism for Deep Inelastic Scattering (DIS) is developped in many texts on particle physics [3,4,5,6,7].

The DIS cross-section can be written as follows:

$$\frac{d^2\sigma}{d\Omega \ dE'} = \frac{\alpha^2}{2M_pQ^4} \frac{E'}{E} L_{\mu\nu} \ W^{\mu\nu} \tag{1}$$

4

Table 1: Kinematic variables relevant to Deep Inelastic Scattering

$(\vec{k}, E)$	Momentum and energy of the incoming lepton
$(\vec{k}', E')$	Momentum and energy of the outgoing lepton
$\nu = E - E'$	Energy transfer in the reaction
$q = k - k'$	Four momentum transfer
$Q^2 = -q^2$	$= 4EE' \sin^2(\theta/2);\;\; \theta$: e$^{\pm}$ scattering angle
$x = Q^2/2M_p\nu$	Fraction of the nucleon momentum carried by the struck quark
$y = \nu/E$	Fraction of the incident energy transferred
$W^2 = M_p^2 + 2M_p\nu - Q^2$	Square of the invariant mass of the photon-nucleon system
$z = E_h/\nu$	Fraction of the energy transferred carried by a particular hadron h
$x_F = 2p_{\parallel}/W$	Scaled longitudinal momentum of a hadron

where α is the fine structure constant and M_p is the mass of the proton. Notice that the cross-section falls off very quickly as a function of momentum transfer Q. $L_{\mu\nu}$ is a tensor which describes the emission of the virtual photon by the lepton; it can be calculated exactly in QED. $W^{\mu\nu}$ is a tensor describing the absorption of the virtual photon by the target; it contains all of the information related to the structure of the target. Symmetry considerations and conservation laws determine the form of $W^{\mu\nu}$:

$$
\begin{aligned}
W^{\mu\nu} \;=\; & -g^{\mu\nu} \cdot \mathbf{F_1} \;\; + \;\; p^{\mu}p^{\nu}/\nu \cdot \mathbf{F_2} \\
& + i/\nu \; \epsilon^{\mu\nu\lambda\sigma} \; q^{\lambda}s^{\sigma} \cdot \mathbf{g_1} \;\; + \;\; i/\nu^2 \; \epsilon^{\mu\nu\lambda\sigma} \; q^{\lambda}(p.q\; s^{\sigma} \; - \; s.q\; p^{\sigma}) \cdot \mathbf{g_2}.
\end{aligned}
\tag{2}
$$

F_1 and F_2 are *unpolarised* structure functions, while g_1 and g_2 are *polarised* structure functions which contribute to the cross-section only if both the target and the beam are polarised. In general, the structure functions depend on ν and Q^2. However, if the scattering occurs from pointlike constituents, they depend only on one variable $x = Q^2/2M_p\nu$. This is the phenomenon of scaling which was the first experimental confirmation that the nucleon is composed of smaller particles. In the infinite momentum frame, x is shown to be the fraction of the nucleon's momentum carried by the struck quark. The structure functions can be interpreted in the quark-parton model in a straightforward way:

$$
F_1(x) = \frac{1}{2} \sum_f e_f^2 \, (q_f^+(x) + q_f^-(x)) \; = \frac{1}{2} \sum_f e_f^2 \, q_f(x)
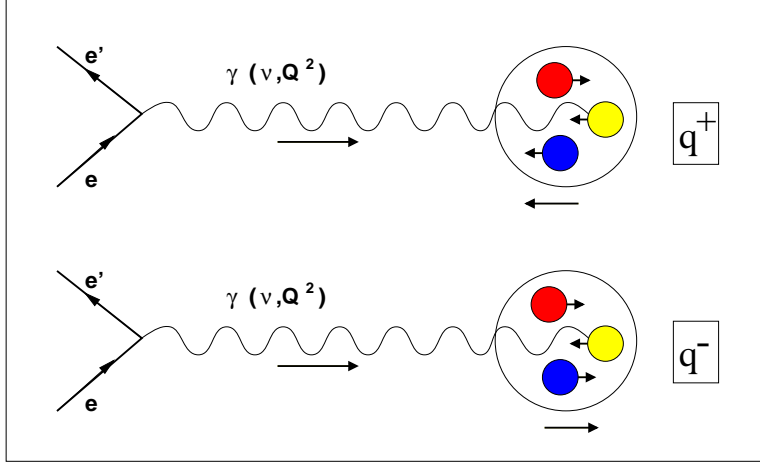\tag{3}
$$

Figure 3: Diagram of Polarised Deep Inelastic Scattering. The virtual photon is always absorbed by a quark with opposite spin direction. The top panel shows the process that is sensitive to quarks polarised parallel to the nucleon's spin ($q_f^+(x)$), while the bottom panel is for quarks with their spin direction anti-parallel to the nucleon ($q_f^-(x)$).

$$g_1(x) = \frac{1}{2} \sum_f e_f^2 \ (q_f^+(x) - q_f^-(x)) \ = \ \frac{1}{2} \sum_f e_f^2 \ \Delta q_f(x) \qquad (4)$$

where the sum is over quark flavours and e_f is the charge of quark. q_f^+ (q_f^-) is the distribution of quarks *and* anti-quarks with their spins in the same (opposite) direction as the spin of the nucleon. $F_1(x)$ measures the momentum distribution of the quarks in the nucleon, while $g_1(x)$ gives the distribution of the spins of the quarks. For spin $1/2$ quarks, F_2 is related to F_1 by [8]

$$F_2(x) = 2xF_1(x). \qquad (5)$$

Finally, $g_2 = 0$ in the quark-parton model since it is related to transverse degrees of freedom which are absent in the simple QPM.

An intuitive picture of how $g_1(x)$ is sensitive to spin degrees of freedom and how to measure it is given in Fig. 3. The incoming polarised lepton at the left emits a circularly polarised virtual photon with spin projection pointing to the right in this picture. This photon can be absorbed only by a quark with spin projection in the opposite direction because the final state (a quark) must have spin $1/2$ and can therefore not have spin projection $3/2$. In the top panel of Fig. 3 the target polarisation 'points' to the left so that we measure
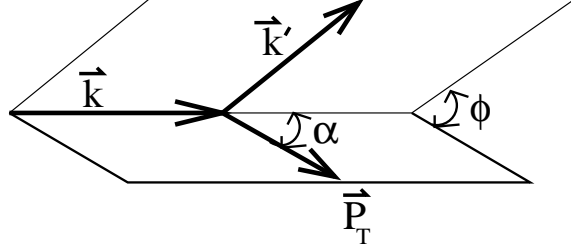
Figure 4: Diagram of the angles relevant to Polarised Deep Inelastic Scattering. See the text for details.

the cross-section for beam and target polarisations anti-parallel. This cross-section is labelled $\sigma^{\uparrow\downarrow}$ and is sensitive to the distribution of quarks with their spins in the same direction as the spin of the host nucleon, or $q_f^+(x)$. In the bottom panel of Fig. 3, the target spin direction has been reversed so that we measure the cross-section for beam and target polarisations parallel ($\sigma^{\uparrow\uparrow}$). However, the elementary process is not changed. The photon absorbs on a quark with spin projection 'pointing' to the left and this process is sensitive to $q_f^-(x)$. Since $g_1(x)$ is related to the difference of $q_f^+(x)$ and $q_f^-(x)$ (see Eqn. 4), it can be deduced by measuring the polarisation asymmetry:

$$A_\parallel = \frac{\sigma^{\uparrow\downarrow} - \sigma^{\uparrow\uparrow}}{\sigma^{\uparrow\downarrow} + \sigma^{\uparrow\uparrow}}. \tag{6}$$

Further insight can be gained into how to measure $g_1(x)$ and $g_2(x)$ by considering Fig. 4. $\vec{k}$ and $\vec{k'}$ are the usual lepton momenta, ϕ is the angle between the lepton scattering plane and the target spin, and α is the angle between the beam and target spins. The target polarisation is said to be longitudinal (transverse) when $\alpha = 0°$ or $180°$ ($= 90°$ or $270°$). The difference in the cross-sections ($\Delta\sigma$) for the two relative directions of the beam and target spins can now be written as follows:

$$\frac{d^3\Delta\sigma}{dxdyd\phi} \propto \cos\alpha \cdot \{a\ g_1(x) + b\ g_2(x)\}$$
$$- \cos\phi\ \sin\alpha \cdot c \cdot \{\tfrac{y}{2}\ g_1(x) + g_2(x)\}. \tag{7}$$

Each of the two terms in braces can be isolated by preparing the target with either longitudinal or transverse target polarisation. The kinematic constants a, b, and c are of order $\mathcal{O}(1)$, $\mathcal{O}(1/Q^2)$, and $\mathcal{O}(1/Q)$ respectively. Therefore, $g_1(x)$ dominates for longitudinal target polarisation, even at moderate Q^2.

This statement is strengthened by the fact that there are good arguments that $g_2(x)$ is small since it is related to transverse degrees of freedom in the nucleon. The small value of $g_2(x)$ has been confirmed by experiment as we will see in Sec. 7.1. Once $g_1(x)$ has been determined, transverse target polarisation can be used to maximize the sensitivity to $g_2(x)$. However, notice that in this case the asymmetry is reduced by the factor $c \propto 1/Q$, making this measurement more difficult.

3.2 What is measured in practice?

This section gives the steps required to go from a measurement of the cross-section asymmetry to the polarised structure functions. First, one must realize that the experimentally observed asymmetry (A_{meas}) is reduced because we do not have perfect beam and target polarisation. It is related to the true asymmetry ($A_\parallel$) by:

$$A_{meas} = \frac{N^{\uparrow\downarrow} - N^{\uparrow\uparrow}}{N^{\uparrow\downarrow} + N^{\uparrow\uparrow}} = (f_D \cdot p_B \cdot p_T) \cdot A_\parallel, \qquad (8)$$

where p_B and p_T are respectively the beam and target polarisations, and f_D is the target dilution factor. f_D is defined as the fraction of polarisable nucleons in the target (1 for H and D gas; $\frac{1}{3}$ for ^{3}He gas; $\frac{3}{17}$ for NH$_3$; and $\frac{10}{74}$ for C$_4$H$_9$OH). f_D is further reduced by extraneous materials in the target such as windows, or vapour introduced for the optical pumping process. Beam polarisations vary from 0.5 to 0.85, while the range of available target polarisations is 0.4-0.9. The ratio of the measured to the real asymmetry is in the range 0.07-0.12 (CERN); 0.17-0.35 (SLAC); 0.25-0.50 (DESY) (see Sec. 8). Since some of the asymmetries are small to begin with, the experiments must be very accurate, requiring high statistics.

The measured asymmetries for longitudinal and transverse target polarisation, corrected for the factors in Eqn. 8, are written in terms of the cross-sections as follows:

$$A_\parallel = \frac{\sigma^{\uparrow\downarrow} - \sigma^{\uparrow\uparrow}}{\sigma^{\uparrow\downarrow} + \sigma^{\uparrow\uparrow}} \quad ; \quad A_\perp = \frac{\hat{\sigma}^{\uparrow\downarrow} - \hat{\sigma}^{\uparrow\uparrow}}{\hat{\sigma}^{\uparrow\downarrow} + \hat{\sigma}^{\uparrow\uparrow}}, \quad \text{where } \hat{\sigma} = \int \frac{1}{\cos\phi} \frac{d\sigma}{d\phi} d\phi. \qquad (9)$$

While $A_\parallel$ and $A_\perp$ depend on beam and target related polarised cross-sections, the physically significant asymmetries for photon absorption on the nucleon level are given by:

$$A_1 = \frac{\sigma_{\frac{1}{2}} - \sigma_{\frac{3}{2}}}{\sigma_{\frac{1}{2}} + \sigma_{\frac{3}{2}}} \quad ; \quad A_2 = \frac{\sigma_{TL}}{\frac{1}{2}(\sigma_{\frac{1}{2}} + \sigma_{\frac{3}{2}})} = \frac{\sigma_{TL}}{\sigma_T}, \qquad (10)$$

where $\sigma_{\frac{1}{2}}$ is the absorption cross-section when the photon and the nucleon have their spins anti-aligned, and $\sigma_{\frac{3}{2}}$ the cross-section when they are aligned. σ_T and σ_{TL} are the absorption cross-section for tranversely polarised virtual photons and the longitudinal-transverse interference respectively.

The measured asymmetries are related to the photon absorption asymmetries by the following equations:

$$A_{\parallel} = D \cdot (A_1 + \eta A_2) \quad ; \quad A_{\perp} = d \cdot (A_2 - \xi A_1). \tag{11}$$

D, η, d, and ξ are depolarisation factors given by:

$$D = \frac{y(2-y)}{y^2 + 2(1-y)(1+R)} \quad ; \quad \eta = \frac{2\gamma(1-y)}{2-y} \quad ; \quad d = D\sqrt{\frac{2\epsilon}{1+\epsilon}} \tag{12}$$

$$\xi = \eta\frac{1+\epsilon}{2\epsilon} \quad ; \quad \epsilon = \frac{1-y}{1-y+\frac{y^2}{2}} \quad ; \quad \gamma = Q/\nu = 2mx/Q.$$

R is the ratio of longitudinal to transverse cross-sections[9]. The depolarisation factors account for the loss of polarisation from the lepton to the virtual photon and depend on kinematics.

Finally, the photon asymmetries are related to the structure functions as follows:

$$A_1 = \frac{g_1 - \gamma^2 g_2}{F_1} \quad ; \quad A_2 = \frac{\gamma(g_1 + g_2)}{F_1}. \tag{13}$$

If g_2 and A_2 are ignored, the equation for g_1 simplifies considerably:

$$g_1(x) \approx F_1(x) \cdot A_1(x) \approx F_1(x) \cdot \frac{A_{\parallel}(x)}{D}. \tag{14}$$

3.3 Data on the Polarised Structure Function $g_1(x)$

The EMC results[10] published in 1988, which indicated that little of the spin of the proton comes from the spins of the quarks, generated a series of experiments at CERN (SMC: H & D targets), SLAC (E142 & 154: ^{3}He, and E143 & 155: H & D), and DESY (HERMES: H, D, & ^{3}He) to study the *"nucleon spin puzzle"*. As a result, we now have precise data on $g_1(x)$ over a range of Q^2. A selection of these data, as of the time of this workshop (Feb.'98), is shown in Figs. 5,6,7 (see the figure captions for references). There are several choices for the form of these plots. Here, the abscissa is plotted on a logarithmic scale to allow the points at low-x to be seen clearly. $xg_1(x)$ rather than $g_1(x)$ is plotted on the ordinate because this is the appropriate quantity to plot to illustrate the contribution of each data point to the integral of $g_1(x)$, the importance of which in terms of the spin content of the nucleon will be discussed in Sec. 4-5.
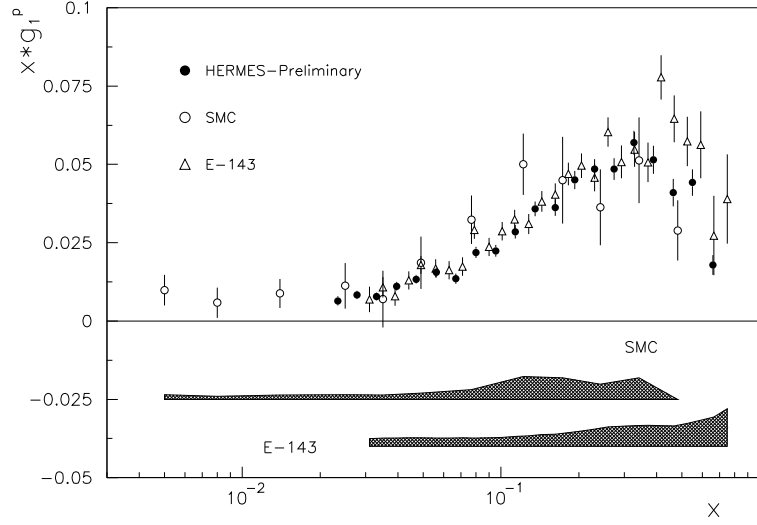
Figure 5: Data on $xg_1^p(x)$ from SMC [11], E143 [14], and preliminary results from HERMES [16]. The E143 data are at $Q^2 = 3$ GeV^2, while the SMC and HERMES data are at the measured Q^2 for each x bin.
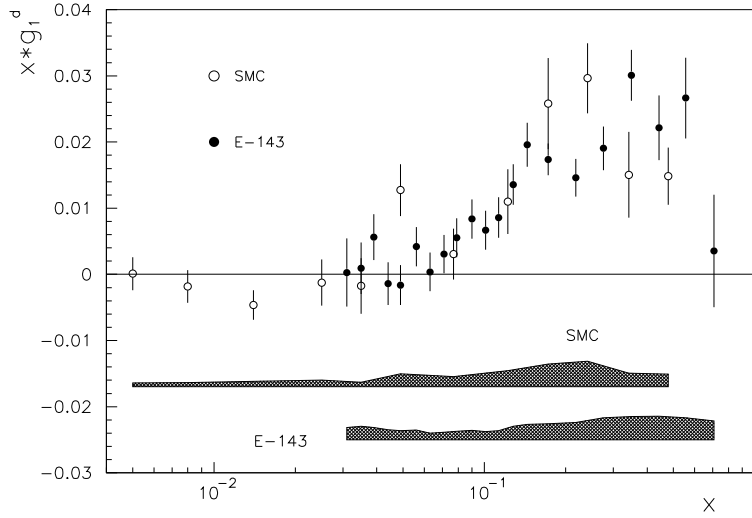

Figure 6: Data on $xg_1^d(x)$ from SMC [12] and E143 [15]. The E143 data are at $Q^2 = 3$ GeV^2, while the SMC data are at the measured Q^2 for each x bin.
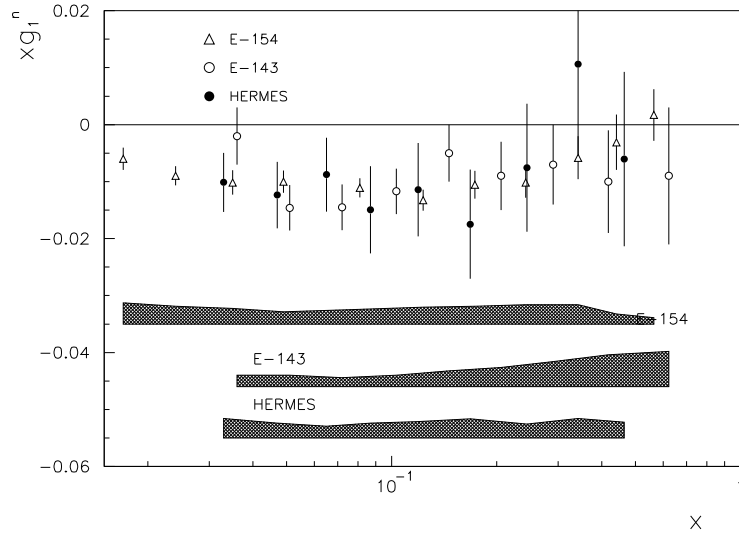
10

Figure 7: Data on $xg_1^n(x)$ from E143 [15], HERMES [17], and E154 [18]. The E143 data are at $Q^2 = 3$ GeV^2, E154 is at $Q^2 = 5$ GeV^2, and the HERMES data are at the measured Q^2 in each x bin.

A few general points can be made about the data. First, although they are taken with widely varying experimental techniques (see Sec. 8), the data are consistent with each other, giving confidence in the results. Second, while the Q^2 varies substantially for the different experiments ($\langle Q^2 \rangle = $ 2-10 GeV^2), $g_1(x)$ shows relatively little Q^2-dependence over most of the x-range, at least within the experimental uncertainties. Third, while the SMC data have worse statistical precision than either the SLAC experiments or HERMES, they extend to lower x which is important for the extrapolation of $g_1(x)$ to $x = 0$. Finally, the precision of the data is quite good and the experiments are now close to being limited by systematic uncertainties.

One should notice that while $g_1^p(x)$ is large and positive for $0.1 < x < 0.6$, $g_1^n(x)$ is small and negative for all x. The reader is referred to the experimental papers for a more complete presentation of the data.

4   The Interpretation of $g_1(x)$ in Terms of Sum Rules

The spin structure functions are often interpreted using sum rules which relate the integrals of $g_1(x)$ over all x to the polarisation of the quarks in the nucleon.

4.1 The Bjorken Sum Rule

If we use Eqn. 4 for the proton and the neutron, we get:

$$\Gamma_1^p = \int_0^1 g_1^p(x)\,dx = \frac{1}{2}\left(\frac{4}{9}\Delta u + \frac{1}{9}\Delta d + \frac{1}{9}\Delta s\right) \tag{15}$$

$$\Gamma_1^n = \int_0^1 g_1^n(x)\,dx = \frac{1}{2}\left(\frac{1}{9}\Delta u + \frac{4}{9}\Delta d + \frac{1}{9}\Delta s\right), \tag{16}$$

where we have used isospin symmetry to make the simplifications:

$$\Delta u_p = \Delta d_n = \Delta u \tag{17}$$
$$\Delta d_p = \Delta u_n = \Delta d \tag{18}$$
$$\Delta s_p = \Delta s_n = \Delta s \tag{19}$$

with the corresponding equations for the anti-quarks. Δu, Δd, and Δs in Eqns. 15, 16 are therefore for the *proton*. The sea cancels in the difference of the two integrals so that

$$\int_0^1 [g_1^p(x) - g_1^n(x)]\,dx = \frac{1}{6}(\Delta u - \Delta d) = \frac{1}{6}\cdot\left|\frac{g_A}{g_V}\right| \tag{20}$$

where the final step comes from neutron β-decay, and g_A and g_V are the axial vector and vector coupling constants. This sum rule, first derived by Bjorken[19] using current algebra, has little model dependence and is fundamental to QCD. If higher order QCD effects are taken into account, the full expression for the *Bjorken Sum Rule* is obtained[20]:

$$\int_0^1 [g_1^p(x) - g_1^n(x)]\,dx = \frac{1}{6}\cdot\left|\frac{g_A}{g_V}\right|\cdot Corr \tag{21}$$

$$Corr = 1 - \left(\frac{\alpha_s(Q^2)}{\pi}\right) - 3.5833\left(\frac{\alpha_s(Q^2)}{\pi}\right)^2$$

$$-20.2153\left(\frac{\alpha_s(Q^2)}{\pi}\right)^3 - \mathcal{O}(130)\left(\frac{\alpha_s(Q^2)}{\pi}\right)^4,$$

where α_s is the Q^2 dependent strong coupling constant. The precise data on $g_1^p(x)$, $g_1^n(x)$, and $g_1^d(x)$ can be used to test the Bjorken sum rule. The current situation is shown in Fig. 8 which is a plot of the neutron integral (Γ_1^n) versus the proton integral (Γ_1^p). The overlap of the bands for the three targets is consistent with the sum rule to one standard deviation. The Bjorken sum rule has been verified to about 10%.
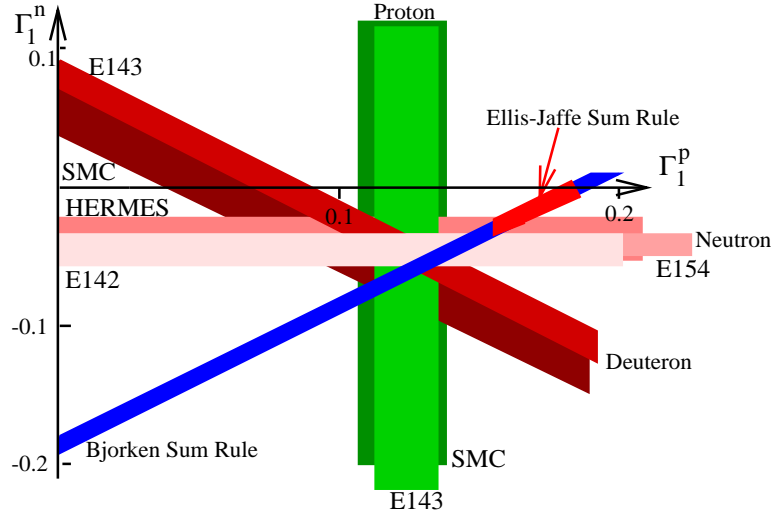
Figure 8: Plot of Γ_1^n versus Γ_1^p. The predictions of the Bjorken and Ellis-Jaffe sum rules are shown on the diagonal band from the lower left to the upper right of the figure. While the data and the Bjorken sum rule overlap within one sigma, the Ellis-Jaffe prediction is roughly two sigma away from the overlap region in the data.

4.2   The Ellis-Jaffe Sum Rules

Because of the difficulty of producing a polarised neutron target, it became clear that data on the proton would be available much before data on the neutron. Ellis and Jaffe [21] derived sum rules for Γ_1^p and Γ_1^n separately using SU(3)$_F$ flavour symmetry and the assumption that $\Delta s = 0$. One can write the following from neutron and hyperon β-decays:

$$\Delta u - \Delta d = F + D \tag{22}$$
$$\Delta u + \Delta d - 2\Delta s = 3F - D$$

where F and D are SU(3)$_F$ coupling constants. If $\Delta s = 0$, we can solve Eqs. 22 for Δu and Δd and write Eqs. 15, 16 in terms of F and D:

$$\int g_1^p(x)\ dx = \frac{1}{18}(9F - D) \tag{23}$$

$$\int g_1^n(x)\ dx = \frac{1}{18}(6F - 4D) \tag{24}$$

13

Table 2: Values of the Ellis-Jaffe integrals from the various polarised DIS experiments. The second number in the fourth column is the statistical uncertainty on the measurement, while the third number is the systematic error.

Experiment	Integral	$\langle Q^2 \rangle$ (GeV^2)	Measurement	Ref.
EMC	Γ_1^p	10.7	$0.114 \pm 0.012 \pm 0.026$	[10]
SMC	Γ_1^p	10	$0.136 \pm 0.013 \pm 0.011$	[11]
	Γ_1^d	10	$0.041 \pm 0.006 \pm 0.005$	[12]
	Γ_1^n	10	$-0.046 \pm 0.018 \pm 0.019$	[12]
E142	Γ_1^n	2	$-0.031 \pm 0.006 \pm 0.009$	[13]
E143	Γ_1^p	3	$0.127 \pm 0.004 \pm 0.009$	[14]
	Γ_1^d	3	$0.042 \pm 0.003 \pm 0.004$	[15]
	Γ_1^n	3	$-0.037 \pm 0.008 \pm 0.011$	[15]
E154	Γ_1^n	5	$-0.041 \pm 0.004 \pm 0.006$	[18]
HERMES	Γ_1^n	2.5	$-0.037 \pm 0.013 \pm 0.008$	[17]

These sum rules are usually written in a different form:

$$\int g_1^p(x)\ dx = \frac{1}{12} \cdot \left| \frac{g_A}{g_V} \right| \cdot \left(1 + \frac{5}{3}\frac{3F-D}{F+D} \right) \times QCD\ Corr. \qquad (25)$$

$$\int g_1^n(x)\ dx = \frac{1}{12} \cdot \left| \frac{g_A}{g_V} \right| \cdot \left(-1 + \frac{5}{3}\frac{3F-D}{F+D} \right) \times QCD\ Corr. \qquad (26)$$

Using the fact that $F + D = g_A/g_V = 1.257 \pm 0.003$ from neutron β-decay and the determination of F/D from a global fit to hyperon β-decays ($F/D = 0.575 \pm 0.016$), we can get numerical predictions for the Ellis-Jaffe integrals. For example [22], at $Q^2 = 5$ GeV^2:

$$\Gamma_1^p(EJ) = 0.172 \pm 0.009 \ ; \ \Gamma_1^n(EJ) = -0.018 \pm 0.009$$

where higher order QCD corrections are included. While the Bjorken sum rule is verified by data, there is significant disagreement between the measured values of Γ_1^p and Γ_1^n and the Ellis-Jaffe predictions. The situation is summarized in Fig. 9 where deviations of several σ can be seen between the data and the predictions. The values of the Ellis-Jaffe integrals for the different experiments are given in Table 2.

The disagreement of the data with the predictions of Ellis and Jaffe is not surprising for several reasons. From the theory standpoint, the assumptions of SU(3)$_F$ symmetry and $\Delta s = 0$ are crude at best. On the experimental side, there is great controversy over how the extrapolation to the unmeasured region
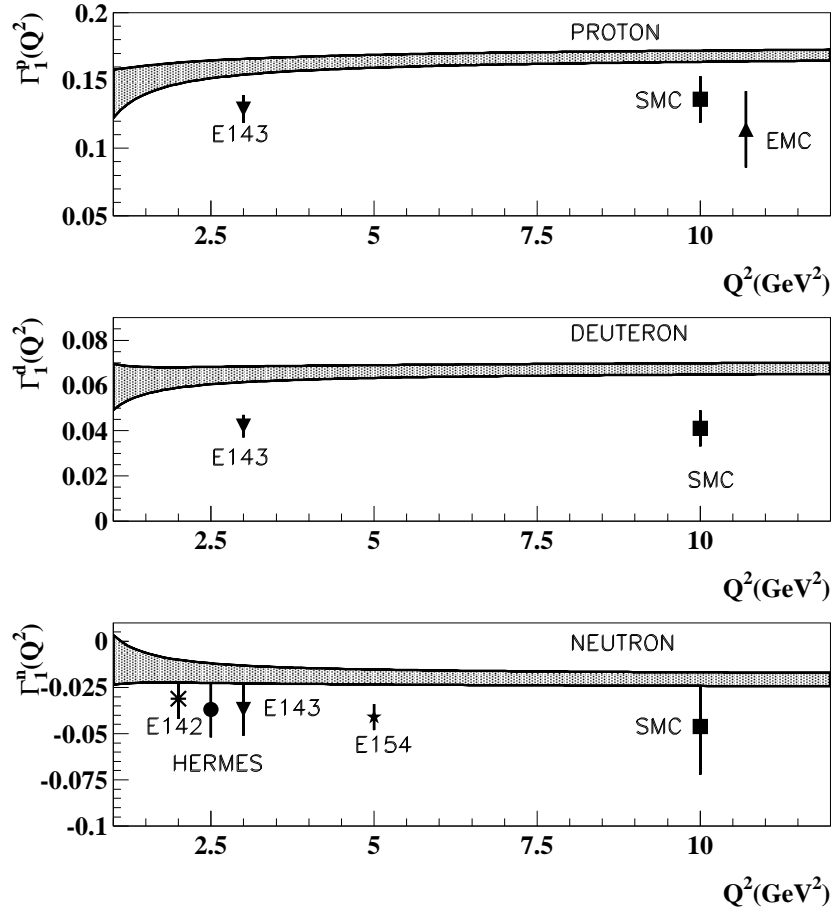
Figure 9: Results for Γ_1^p, Γ_1^n, and Γ_1^d compared to the predictions of Ellis and Jaffe (shaded area).

at low x should be done. Regge theory has been used in the past but recent low x data (F_2 and g_1) have shown this to be inappropriate. Several other functions have been tried in the low x region but there is no agreement to date on the proper form to use (see for example Ref. [23] and references therein).

5   The Spin Content of the Nucleon

The expressions for the integrals Γ_1^p and Γ_1^n, and for the matrix elements of hyperon β-decays in terms of Δu, Δd, and Δs can be used to deduce the fraction of the nucleon spin due to the spins of the quarks. In practice, global fits are made to all the data. However as an illustration, a simple example is shown here which has the added advantage of giving historical insight into the *'Spin Crisis'* since it uses the original EMC data [10]. Consider the following system of three equations and three unknowns:

$$\Gamma_1^p = \frac{1}{2}(\frac{4}{9}\Delta u + \frac{1}{9}\Delta d + \frac{1}{9}\Delta s) = 0.114 \pm 0.029 \quad (EMC)$$
$$\Delta u - \Delta d = 1.257 \pm 0.011 \quad (\text{neutron } \beta - \text{decay}) \tag{27}$$
$$\Delta u + \Delta d - 2\Delta s = 0.579 \pm 0.016 \quad (\text{hyperon } \beta - \text{decay}).$$

Solving for Δu, Δd, and Δs, we get:

$$\Delta u = 0.705 \pm 0.09 \;\; ; \;\; \Delta d = -0.553 \pm 0.09 \;\; ; \;\; \Delta s = -0.214 \pm 0.09. \tag{28}$$

The total contribution to the nucleon's spin from the quark spins is therefore

$$\Delta\Sigma = \Delta u + \Delta d + \Delta s = -0.062 \pm 0.16, \tag{29}$$

consistent with 0 and several standard deviations from what was expected. The EMC did a somewhat different analysis (assuming the validity of the Bjorken sum rule) but they also obtained $\Delta\Sigma \approx 0$. This surprising result lead to the new round of experiments designed specifically for polarised DIS. Now that many more data exist, global fits are done to get the Δq's with resulting values of $\Delta\Sigma$ in the range 0.2-0.3, still significantly below expectation.

In the naive quark parton model, all the spin of the nucleon comes from the spin of the quarks so that $\Delta\Sigma = 1$. If relativistic wave functions are used

$$\psi = \left[\begin{array}{c} \chi \\ \frac{\sigma \cdot p}{E+m} \cdot \chi \end{array} \right],$$

the lower components contribute orbital angular momentum and $\Delta\Sigma$ is reduced to 0.75 [5]. The Ellis-Jaffe prediction for $\Delta\Sigma$ can be obtained from Eqn. 22 with $\Delta s{=}0$:

$$\Delta u + \Delta d = 3F - D \quad \Rightarrow \quad \Delta\Sigma = 3 \times 0.459 - 0.791 = 0.586.$$

It is clear that no matter what one does, the measurements of $\Delta\Sigma$ are all in disagreement with the predictions indicating that there is still something we do not understand about the spin of the nucleon; or that there is something wrong with our interpretation of $\Delta\Sigma$ (see below).

6 The Q^2 Evolution of the Structure Functions

6.1 Alternate expression for $g_1(x)$

Eqns. 4, 15, and 16 give simple expressions for $g_1(x)$ in term of the quark distributions. These can be generalized to include gluons and written in a form which is convenient for the Q^2 evolution of the structure functions[24]:

$$g_1(x, Q^2) = \frac{\langle e^2 \rangle}{2} \; [C_{ns} \otimes \Delta q_{ns} + C_s \otimes \Delta\Sigma + 2n_f \; C_g \otimes \Delta g], \qquad (30)$$

$$\text{where} \quad \langle e^2 \rangle \quad = \quad \frac{1}{n_f} \sum_{i=1}^{n_f} e_i^2, \qquad (31)$$

$$\Delta q_{ns} \quad = \quad \sum_{i=1}^{n_f} \left(\frac{e_i^2}{\langle e^2 \rangle} - 1 \right) (\Delta q_i + \Delta\bar{q}_i) \qquad (32)$$

$$= \quad \frac{3}{5}(\Delta u - \Delta d) \; \text{(for 2 flavours)}, \quad \text{and}$$

$$\Delta\Sigma \quad = \quad \sum_{i=1}^{n_f} (\Delta q_i + \Delta\bar{q}_i). \qquad (33)$$

Δq_{ns} is called the *non-singlet* quark distribution, $\Delta\Sigma$ is the *singlet* quark distribution, Δg is the gluon polarisation, n_f is the number of quark flavours, and C_{ns}, C_s, and C_g are coefficient functions calculable in QCD. The $\otimes$ in Eqn. 30 refers to a convolution defined as follows:

$$(C \otimes q)(x, Q^2) = \int_x^1 C \left(\frac{x}{z}, \alpha_S \right) q(z, Q^2) \frac{dz}{z}. \qquad (34)$$

The advantages of this formulation can be seen if one considers the evolution of g_1 with Q^2. This evolution is given by the DGLAP equations[25]:

$$\frac{d}{dt} \Delta q_{ns} = \frac{\alpha_s(t)}{2\pi} \; P_{qq}^{ns} \otimes \Delta q_{ns} \quad ; \quad t = log \left(\frac{Q^2}{\Lambda^2} \right) \qquad (35)$$

$$\frac{d}{dt} \left(\begin{array}{c} \Delta\Sigma \\ \Delta g \end{array} \right) = \frac{\alpha_s(t)}{2\pi} \left(\begin{array}{cc} P_{qq}^s & 2n_f P_{qg}^s \\ P_{gq}^s & P_{gg}^s \end{array} \right) \otimes \left(\begin{array}{c} \Delta\Sigma \\ \Delta g \end{array} \right). \qquad (36)$$

17

P_{qq}^{ns} and the P_{ij}^s are splitting functions and Λ is the constant of the strong interaction ($\approx$ 200-300 MeV). The first thing to notice is that the Q^2 evolution of the non-singlet term does not depend on the gluons. Since the Bjorken sum rule is related to the non-singlet term (see Eqns. 20, 32), it depends only on the quark distributions. On the other hand, the evolution of the singlet term depends on both the quark and gluon distributions. Therefore, we must be very careful in our interpretation of $\Delta\Sigma$. In fact, the quark distributions as measured in DIS ($\Delta\tilde{q}$) are modified by a gluon term Δg[26]:

$$\Delta\tilde{q} = \Delta q - \frac{\alpha_s n_f}{2\pi}\,\Delta g. \tag{37}$$

n_f is the number of active quark flavours (3 if heavy quarks are ignored). This is thought to be the best candidate to explain the relatively small measured value of $\Delta\Sigma$, and the search for an indication that the gluons are polarised has become a focus of the field.

### 6.2   Gluon Polarisation from Q^2 Evolution

There have been attempts to extract a value of Δg from the Q^2 evolution of $g_1(x)$ by using Eqns. 30, 35, and 36 to perform a global fit to data at different Q^2. The result of these fits for the E143 data[27] is shown in Fig. 10 where some Q^2 dependence is seen at low Q^2, albeit small. Values of Δg in the range 1.5-2.0 have been deduced in several studies[24,28,29,30]. However, the uncertainties are large and the data are consistent with Δg=0. Much better data will be required for this technique to produce reliable results.

7   Other Structure Functions

7.1 $g_2(x)$

Until now the discussion has centered on g_1. However, several other structure functions can be measured. $g_2(x)$ has already been introduced in Eqn. 2 and Sec. 3.2. While g_2 could be important as a correction to g_1, it is also interesting in its own right because it could offer a way of isolating the effects of a twist-3 operator[31]. Twist is a number that arises in the operator product expansion and is an indication of the order of the operator involved[32]. Twist-2 operators are leading-order, while twist-3 are next-to-leading order, etc. The following expression for g_2 shows a term ($\tilde{g}_2$) which is pure twist-3:

$$g_2(x, Q^2) = g_2^{WW}(x, Q^2) + \tilde{g}_2(x, Q^2) \tag{38}$$

18
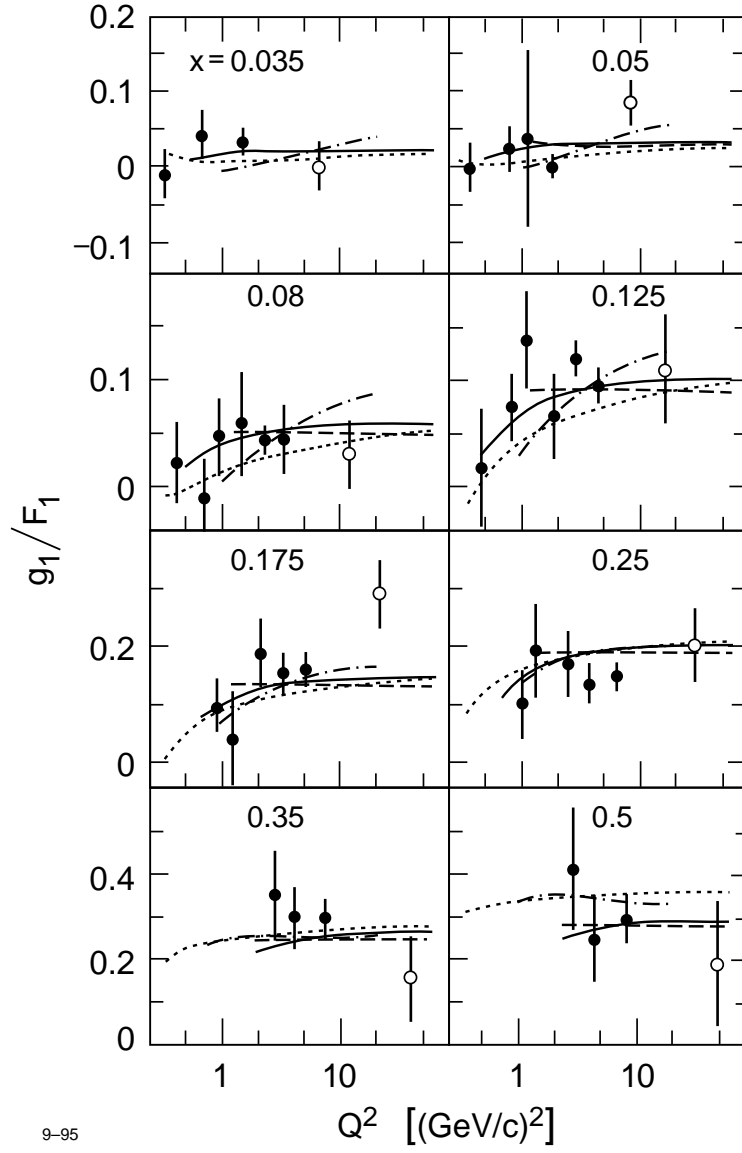
Figure 10: g_1^d/F_1^d as a function of Q^2 in separate x bins. The curves are different global fits to the asymmetries. This figure is taken from Ref. [27] where more detail can be found on the fits.
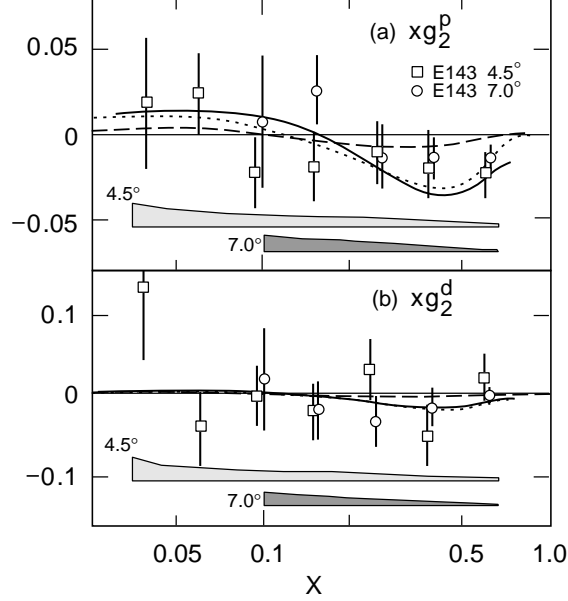
19

Figure 11: Measurements of (a) xg_2^p and (b) xg_2^d from E143 at SLAC [34]. Systematic uncertainties are indicated by the bands. The solid curve shows the g_2^{WW} calculations. Bag model calculations at $Q^2 = 5.0$ GeV^2 by Stratmann [35] (dotted), and Song and McCarthy [36] (dashed) are also shown.

$$\text{with} \quad g_2^{WW}(x, Q^2) = -g_1(x, Q^2) + \int_x^1 \frac{g_1(y, Q^2)}{y}\, dy \qquad (39)$$

The term g_2^{WW} was derived by Wandzura and Wilczek [33]. It is twist-2 (i.e. leading order) and can be calculated from g_1. A deviation of g_2 from g_2^{WW} would signal the effect of a twist-3 operator. Data on g_2 from SLAC [34] are shown in Fig. 11. The data are consistent with either 0 or g_2^{WW} which is shown as the solid line. They are not precise enough to distinguish between these two possibilities or to isolate any possible twist-3 contribution. However, these data confirm that corrections to g_1 due to g_2 are small. More precise data on g_2 are expected from SLAC in 1999.

Burkhart and Cottingham [37] have derived a sum rule for g_2:

$$\int_0^1 g_2(x)\, dx = 0 \qquad (Q^2 \to \infty). \qquad (40)$$

20

The data in Fig. 11 have been integrated with the following results[34]:

$$\int_{0.03}^{1} g_2^p(x)\, dx = -0.013 \pm 0.028 \tag{41}$$

$$\int_{0.03}^{1} g_2^d(x)\, dx = -0.033 \pm 0.082 \tag{42}$$

both consistent with 0.

7.2   Still more Structure Functions

$h_1(x)$

$h_1(x)$ is a twist-2 structure function like $F_1(x)$ and $g_1(x)$ [38]. It is related to tensor currents in the nucleon. However, it is more difficult to measure because it is chiral-odd. A longitudinally polarised beam and a transversely polarised target are needed to measure $h_1(x)$. Furthermore, because this structure function is chiral-odd, pions must be detected in coincidence with the lepton to conserve chirality.

$b_1(x)$

$b_1(x)$ is measured with an unpolarised beam and a longitudinaly polarised D target in each of three substates (m_d= 1, 0, –1). It is given by the expression:

$$b_1(x) = \frac{1}{2} \sum_f e_f^2 \left[q_f^+(x) + q_f^-(x) - 2q_f^0(x) \right] \tag{43}$$

and measures quarks from nuclear binding[39].

$\Delta(x)$

$\Delta(x)$ is also measured with an unpolarised beam and a D target, but in this case the target is transversely polarised in the m_d=0 state. The ϕ distribution of the scattered leptons determines $\Delta(x)$ which is sensitive to gluons not identified with individual nucleons[40].

8   Experiments to Study the Spin Structure of the Nucleon

We will now spend some time describing the recent experiments which have studied polarised deep inelastic scattering. The emphasis will be on the unique features of each one.
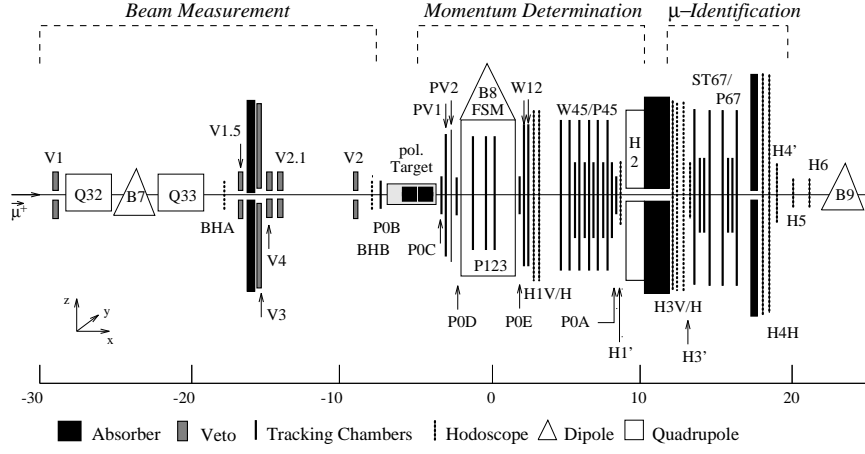
Figure 12: SMC Spectrometer.

8.1   CERN: The Spin Muon Collaboration (SMC)

In the SMC experiment, 100-190 GeV muons scatter from butanol ($C_4\vec{H}_9O\vec{H}$), deuterated butanol ($C_4\vec{D}_9O\vec{D}$), and ammonia ($N\vec{H}_3$) targets (see Ref. [11] and references therein). The experiment is an extension of the pioneering work done at CERN in the eighties and uses essentially the same spectrometer as the EMC, shown in Fig. 12. This device is centered around a large aperture dipole magnet which provides a 2.3 T.m magnetic field. Particle tracks are determined by a series of multi-wire proportional chambers and drift chambers. Muon identification is done using a thick hadron absorber behind the tracking chambers, followed by streamer tubes. The trigger is generated by three hodoscopes behind the absorber.

The muon beam is produced by the decay in flight of pions and kaons. The current is equivalent to about 0.5 pA (4.5×10^7 muons per spill in 2.4 s every 14.4 s). The muons are polarised because of parity violation in the pion and kaon decays. The typical beam polarisation was 80%, determined by a calculation and confirmed by a measurement of the Michel spectrum of μ decays downstream of the experiment.

The target is polarised using dynamic nuclear polarisation. In this technique, the high polarisation of electrons in paramagnetic impurities is trans-

Table 3: Running conditions for SMC.

Year	E_B (GeV)	p_B	p_T	f_D	Target
'92	100	0.84	0.35	0.23	d-butanol
'93	190	0.79	0.86	0.13	p-butanol
'94	190	0.79	0.50	0.23	d-butanol
'95	190	0.79	0.50	0.23	d-butanol
'96	190	0.79	0.89	0.17	p-NH$_3$

ferred to protons using simultaneous flips of these spins induced by microwave irradiation. The polarisation direction is chosen by adjusting the frequency of the microwaves. The target operates in a high magnetic field (2.5 T) at a temperature of 50 mK. The target orientation can be chosen longitudinal or transverse to the incoming muon. One of the remarkable features of the experiment is that two targets with opposite spin direction are used simultaneously. Each target cell is 60 cm long and 5 cm in diameter. The use of two targets is ideal for measuring yield ratios and asymmetries, greatly reducing the systematic uncertainties related to luminosity and detector performance. On the other hand, the SMC targets have the disadvantage of containing a large fraction of unpolarised nucleons which greatly dilutes the experimentally observed asymmetry. A measure of this effect is given by the *dilution factor* f_D which is the ratio of polarisable nucleons divided by the total number of nucleons in the target. The factor f_D varies from 0.13 to 0.23 in the SMC experiment. The polarisation of each half of the target is flipped from time to time to take into account the difference in the acceptance of the spectrometer for each target section. The polarisation is measured using NMR and was found to be $\approx 86\%$ for protons and 25-50% for deuterons. Target thicknesses of about $5 \cdot 10^{24}$ cm^{-2} were obtained leading to luminosities on the order of $1\text{-}2 \cdot 10^{31}$ cm^{-2} s^{-1}. The running conditions for SMC from 1992 to 1996 are summarised in Table 3.

Another unique feature of SMC is that it has the highest beam energy of the polarised DIS experiments and therefore the highest Q^2 ($\langle Q^2 \rangle \approx 10$ GeV^2) and lowest x ($x_{min} \approx 0.003$). The low x points are especially valuable in determining the best functional form to use for the extrapolation of $g_1(x)$ to $x = 0$.

The SLAC experiments use spectrometers in end-station A. While the technology used for the polarised electron beam is the same for all these experiments, the targets are very different (see references in [13] for more details).

The beam is produced by photoemission from an AlGaAs crystal induced by circularly polarised laser light. The direction of the electron spin is chosen at random on a pulse by pulse basis. The beam polarisation is measured by Møller scattering from thin ferromagnetic foils. It was about 36% for E142 and improved dramatically for the subsequent experiments to 82-86% by using a strained AlGaAs crystal. The beam energy varied from 9.7-29.1 GeV for E142-143 to 48.3 GeV for E154. Beam currents also varied from 0.5-3.5 μA (e.g. 2.10^{11} e^- per pulse with a 120 Hz repetition rate for E142, to $3-9.10^{10}$ e^- per pulse for E154).

E142 and E154 used a $^3\vec{\text{He}}$ target [13], while E143 and E155 used $\text{N}\vec{\text{H}}_3$, $\text{N}\vec{\text{D}}_3$ and $\text{Li}\vec{\text{D}}$ targets. As discussed in Sec. 2.1, any spin effects observed in ^3He scattering can be ascribed to the neutron. The SLAC target uses optical pumping by infrared lasers of Rb atoms, followed by spin-exchange with the ^3He nuclei. Two cells are used, one for optical pumping and one for the scattering, connected by a thin tube. This helps reduce the amount of Rb in the beam which in turn keeps the dilution factor f_D relatively high ($f_D \approx 0.33$ for E142). The target cell was 30 cm long by 2 cm in diameter and contained between 8.4 atm (E142) and 9.5 atm (E154) of gas at 20°C. The polarisation, measured using NMR, was 33% for E142 and 38% for E154. The target polarisation was reversed from time to time to reduce the systematic uncertainty in the asymmetry. The $\text{N}\vec{\text{H}}_3$ and $\text{N}\vec{\text{D}}_3$ targets used by E143 and E155 ($\text{Li}\vec{\text{D}}$ instead of $\text{N}\vec{\text{D}}_3$) are similar to the SMC target in that they also use dynamic nuclear polarisation. However, in this case only one target cell is used and it is much smaller than the SMC target (3 cm long and 2.5 cm in diameter). The target field is 4.8 T and the temperature is 1.6 K. The polarisations were in the range 65-80% for the proton and $\approx$25% for the deuteron. The dilution factors range from 0.17 (H) to 0.25 (D). The advantage for E155 of $\text{Li}\vec{\text{D}}$ over $\text{N}\vec{\text{D}}_3$ comes from the fact that the Li, which can be described approximately as an α-particle plus a deuteron, is also polarised. Hence the dilution factor is better for $\text{Li}\vec{\text{D}}$.

The spectrometers used for E142-143 are shown schematically in Fig.13. The electrons are detected at scattering angles of 4.5° and 7.0°. The spectrometers were modified for operation at higher energy for E154-155. In particular, the scattering angles were changed to 2.75° and 5.5° and a new 10° spectrometer was built. Electrons are identified by Čerenkov detectors and lead-glass
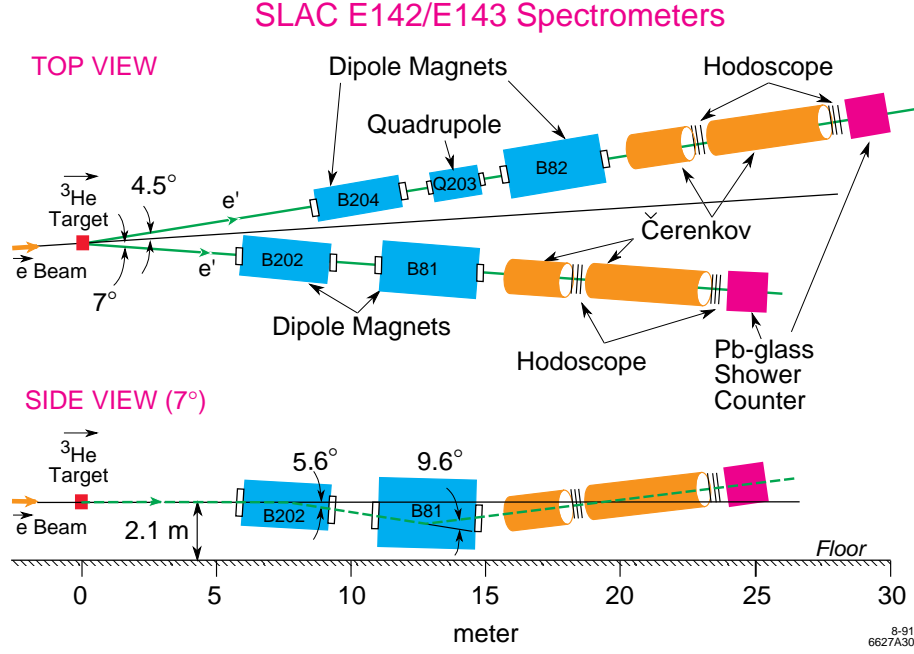
Figure 13: Spectrometer for SLAC Experiments E142 and E143.

calorimeters while tracking is done with scintillator hodoscopes. The geometrical acceptance of these spectrometers is small compared to the other experiments.

The running conditions for the SLAC experiments are summarized in Table 4.

8.3 DESY: HERMES

The HERMES experiment uses a polarised positron (electron) beam and pure gas targets internal to the HERA storage ring. The beam energy is 27.5 GeV and typical currents range from 40 mA at the start of a machine fill to 10-12 mA when the beam is dumped. The positrons are polarised after acceleration using the Sokolov-Ternov effect [41]. This takes advantage of a small asymmetry in the spin-flip amplitude in the emission of synchrotron radiation. Polarisation builds up over a period of roughly half an hour to an equilibrium level between 55% and 60%. The polarisation which is transverse to the beam momentum is rotated into the longitudinal direction in the HERMES straight section by

25

Table 4: Running conditions for the SLAC experiments.

Experiment	E_B (GeV)	p_B	p_T	f_D	Target
E142	19-26	0.36	0.33	0.33	^{3}He
E143	9.7-29.1	0.85	0.7 (H)	0.17 (H)	NH_3
			0.25(D)	0.25 (D)	ND_3
E154	48.3	0.82	0.38	0.55	^{3}He
E155	48.3	0.8	0.83(H)	0.23	NH_3
			0.23(D)	0.23	LiD

a series of magnets. It is rotated back to transverse downstream of the experiment. The beam polarisation is measured using Compton backscattering of circularly polarised laser light [42]. HERA is an e-p collider and while the proton beam is not used by HERMES, it nonetheless goes through the experiment, displaced horizontally by 72 cm from the positron beam.

One of the strengths of HERMES is the purity of the targets. The dilution factor is 1 (the maximum of 1/3 for ^{3}He) so that the experimentally observed asymmetry is not quenched. Polarised gases (H, D, ^{3}He) flow into a windowless storage cell in the beam pipe. The cell has an elliptical cross-section (9.8 mm high × 29 mm wide) and is 400 mm long. It increases the areal density of the target by two orders of magnitude compared to a free atomic beam. Gas escapes out of the ends of the cell and is pumped away by a high speed differential pumping system. The $^3\vec{\mathrm{He}}$ target is polarised by optical pumping [43]. However, in contrast to the SLAC target, the ^{3}He is pumped directly so there are no extraneous atomic species to dilute the target. The ^{3}He nuclei are polarised by spin exchange collisions with ^3S metastable ^{3}He atoms in a glass cell. The ^3S atoms are produced by a weak RF discharge and polarised by optical pumping with 1083 nm laser light. The target thickness is limited to 10^{15} nucleons/cm^2 by the requirement that the lifetime of the positron beam not be affected significantly by the target. The polarisation is measured by optical means and averaged 50% in 1995. The $\vec{\mathrm{H}}$ and $\vec{\mathrm{D}}$ targets are produced by an atomic beam source (ABS) based on the Stern-Gerlach effect to select specific spin states. The thickness of the H target was $\approx 7.10^{13}$ atoms/cm^2. The polarisation is measured by sampling the gas in the cell with a Breit-Rabi polarimeter which determines the fraction of atoms in each substate. Polarisations as high as 92% were measured. However, recombination of atoms into molecules and depolarisation by collisions with the cell walls reduces this to $\approx 88\%$ when averaged over all atoms in the cell.

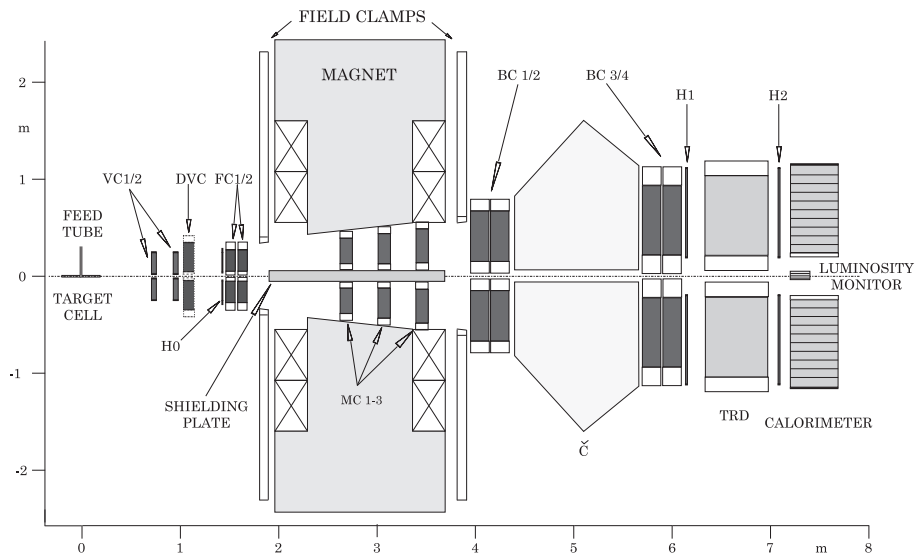The HERMES detector [44] is a forward spectrometer with a large aperture

26

Figure 14: HERMES Spectrometer.

dipole magnet which provides a field of 1.3 T.m (see Fig. 14). A horizontal iron plate shields the beams from the magnetic field. The spectrometer is therefore divided into two identical halves. Micro-strip gas chambers just downstream of the target exit window and drift chambers before and after the magnet measure the scattering angle and momentum of charged particles. Proportional chambers inside the magnet track low momentum particles that do not reach the rear of the spectrometer. This is particularly valuable for pions from Λ decays. Particle identification is provided by a lead-glass calorimeter preceded by a pre-shower detector, a six-module transition radiation detector, and a threshold Čerenkov detector which is used primarily for pion identification. The Čerenkov detector has been upgraded to a dual radiator (C_4F_{10}/aerogel) RICH during the 1997-98 shutdown. This will allow π-K-p separation over almost all of the kinematic range of the experiment (2-20 GeV). The large acceptance of the spectrometer makes it possible to detect hadrons in coincidence with the scattered positron allowing HERMES to make the semi-inclusive measurements described in section 9 which are the cornerstone of the HERMES physics program.

The running conditions at HERMES are summarized in Table 5.

27

Table 5: Running conditions for HERMES.

Year	E_B (GeV)	p_B	p_T	f_D	Target
'95	27.5	0.5	0.50	1/3	^{3}He
'96	27.5	0.55	0.80	1	H
'97	27.5	0.55	0.88	1	H
'98*	27.5	0.55*	0.85*	1	D
'99*	27.5	0.55*	0.85*	1	D

* Planned

9   Semi-inclusive Deep Inelastic Scattering

9.1   The Next Step towards Understanding the Spin of the Nucleon

The experimental activity of the last decade has produced precise data for *inclusive* polarised DIS and can be summarized by the following statements:

- The EMC result for the integral of $g_1^p(x)$ has been confirmed.

- The Bjorken sum rule has been verified to about 10%.

- The integrals of $g_1^p(x)$, $g_1^n(x)$, and $g_1^d(x)$ disagree with the Ellis-Jaffe predictions by up to several standard deviations.

- The quark spins could contribute as little as 20% of the total nucleon spin.

- The nucleon spin puzzle is not yet solved.

The spin of the nucleon can be broken down into four components:

$$S_z = \frac{1}{2} \left(\Delta V + \Delta S \right) + \Delta g + L_z \tag{44}$$

where ΔV is the contribution from the valence quarks, ΔS comes from the sea quarks, Δg is the gluon polarisation, and L_z is a possible contribution from the orbital angular momentum of the partons. Inclusive polarised DIS is sensitive mainly to $(\Delta V + \Delta S)$. Since the quality of the inclusive data sets is now very good, further progress towards a solution to the spin problem must come from qualitatively different data, in particular hadrons produced in coincidence with the scattered lepton. Some information on Δg can be obtained from the Q^2 evolution of $g_1(x, Q^2)$ but we have seen that these effects are small and that the current data are not precise enough to lead to a reliable result.

The strength of the semi-inclusive measurements is that the type of hadron detected gives information on the flavour of the struck quark [45,46]. This is called *flavour tagging*. For example, a high energy π^+ coming from a $e^+ - p$ collision was likely produced by the fragmentation of a u quark. This allows the spin distributions of particular quark flavours to be determined and terms in Eqn. 44 to be isolated. Some examples of this are discussed in later sections. Briefly:

ΔV: The valence quark distributions can be derived from data on the charge dependent polarisation asymmetry in pion production (Sec. 9.4).

ΔS: The light sea quark distributions can be determined from the polarisation asymmetry of π^- production. π^- is a $d\bar{u}$ bound state. Since the charge of the $\bar{u}$ is twice that of the d, it dominates the cross-section (remember the e_q^2 term) and this process is sensitive to the light sea. Information on the strange sea can be obtained from K^- production since it is a $\bar{u}s$ state (Sec. 9.4).

Δg: The photon-gluon fusion process dominates the production of charm particles in DIS. Information on Δg can therefore be obtained from the polarisation asymmetry in J/ψ and D^0 production (Sec. 9.6).

L_z: It has been proposed that the orbital angular momentum contribution to the nucleon's spin might be deduced from an azimuthal asymmetry in hadron production with a transversely polarised target. However, this is still controversial.

9.2 Kinematics; the Current and Target Regions

Two new variables are used to characterize hadrons as coming either from the struck quark (*current region*) or from the target remnant (*target region*):

$$z = \frac{E_h}{\nu} \quad ; \quad x_f = \frac{2p_\parallel}{W}. \tag{45}$$

z is the fraction of the energy transferred in the DIS process (ν) carried by the hadron, and x_F (x-Feynman) is a measure of the longitudinal momentum of the hadron in the $\gamma^* - p$ reference frame. Current quarks tend to produce hadrons at high z and positive x_F, while the target region is characterized by low z, negative-x_F hadrons. We will see later that we are interested primarily in hadrons produced by current quarks.

The question of how high in z is enough to ensure that the hadron comes from the current quark is not trivial. Surely $z > 0.5$ is safe but most hadrons
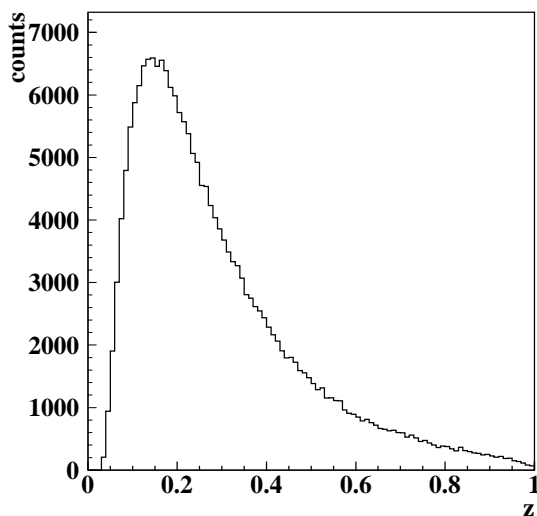
Figure 15: z-distribution of hadrons at HERMES in 1996.

are produced below $z = 0.5$ (see Fig. 15) and lowering the cut on z is necessary to obtain a sufficient number of events. This problem was studied by Berger who defined criteria to ensure that a given hadron came from the current quark [47]. He considered the rapidity:

$$y_h = \frac{1}{2} \log \left(\frac{E_h + p_{h,\parallel}}{E_h - p_{h,\parallel}} \right) \tag{46}$$

and used the experimentally observed fact that the typical hadronic correlation length in a jet is 2 units of rapidity. In other words, it is highly unlikely that two jets separated by $\Delta y_h \geq 4$ will contain hadrons coming from each other. Since the maximum range in y_h which is kinematically allowed for a jet is

$$Y = \log W^2 = \log \left(Q^2 \, \frac{1-x}{x} \right), \tag{47}$$

the condition $Y \geq 4$ translates to $W \geq 7.4$ GeV. Therefore, if we look along the direction of the virtual photon and apply Berger's criterion, we are reasonably assured that we are looking only at hadrons from current quarks. However, it is important to realise that this criterion need only be satisfied if we want

30

to consider *all values* of z. The condition on W can be relaxed if a cut on z is used. For example, for $Y \geq 2$ (i.e. $W \geq 3$ GeV) it is likely that the hadron which is carrying the most energy (called the *leading hadron*) comes from the current quark. Another useful guideline is that for $z \geq 0.2$, we need only require $W \geq 4.8$ GeV.

In practice, the best way to be sure that contamination from the target region is not significant is to determine the quantity of interest with varying cuts on z and show that the result is stable.

9.3 *Factorisation and the Semi-inclusive Cross-Section*

The multiplicity of hadron h in the final state is given by:

$$\frac{1}{\sigma_{tot}} \, \frac{d^3\sigma_h}{dx \, dQ^2 dz} = \frac{\sum_i e_i^2 \, q_i(x, Q^2) \, D_i^h(z, Q^2)}{\sum_i e_i^2 \, q_i(x, Q^2)} \tag{48}$$

where the sum is over quarks and anti-quarks separately. σ_{tot} is the inclusive cross-section, e_i is the charge of the struck quark, $q_i(x, Q^2)$ are the quark distribution functions, and $D_i^h(z, Q^2)$ are the fragmentation functions. $D_i^h(z, Q^2)$ is the probability density that a quark i will produce hadron h with energy $z\nu$ when it undergoes the process of fragmentation as it leaves the nucleon [48]. In other words, Eqn. 48 tells us that the mean number of hadrons h produced is a convolution of the probability to strike a quark q_i and the likelihood that this quark will fragment into hadron h. In principle, the fragmentation functions depend on Q^2 as well as z but this is a relatively small effect and is ignored in most of what follows. Q^2 effects in fragmentation are studied as corrections to the final results.

Implicit in Eqn. 48 is the concept of *factorisation*. This means that the fragmentation process is independent of the hard process that produced the outgoing quark, which in DIS is the absorption of the virtual photon by the struck quark. In practice, this means that in Eqn. 48 the fragmentation functions depend only on z. This leads to the remarkable fact that the fragmentation functions measured in $e^+ - e^-$ collisions should be the same as those measured in DIS. This has been verified experimentally [49]. Also assumed in Eqn. 48 is that the hadrons observed are from current quarks. If the latter condition is not met then factorisation might appear to be broken.

Ultimately, the best way to be sure that factorisation holds is to plot an x-dependent quantity as a function of z and show that it is independent of this variable. The same can be done for z-dependent functions in terms of their x-dependence.
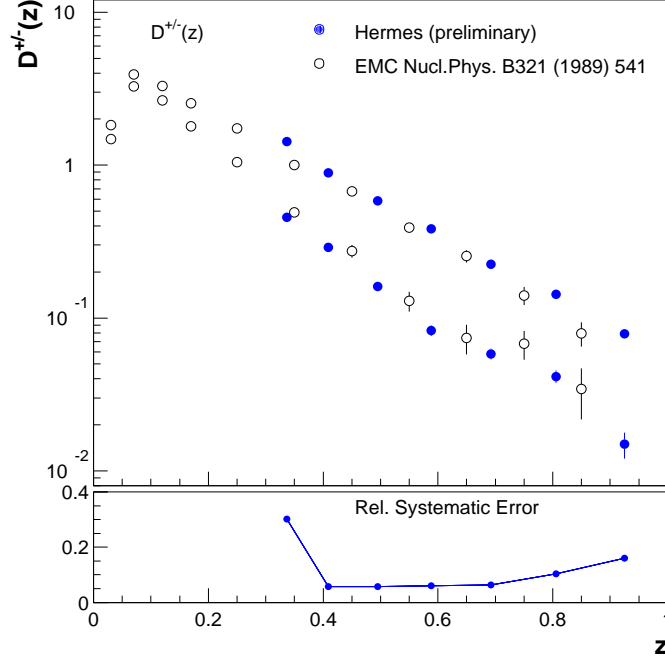
Figure 16: Favoured (D_1) and unfavoured (D_2) fragmentation functions from HERMES[50] (filled circles) and EMC[51] (open circles). The EMC data have been evolved to the same Q^2 as HERMES (2.35 GeV^2).

Some simplifying assumptions can be used to reduce the number of terms in Eqn. 48. For example, consider $\pi^\pm$ production on the proton. Even if only three quark flavours (u, d, and s) are included, we have 12 fragmentation functions. Using isospin symmetry and charge conjugation invariance, we can make the following simplifications:

$$D_1 = D_u^{\pi^+} = D_{\bar{d}}^{\pi^+} = D_d^{\pi^-} = D_{\bar{u}}^{\pi^-} \qquad \text{(Favoured FF)} \qquad (49)$$

$$D_2 = D_d^{\pi^+} = D_{\bar{u}}^{\pi^+} = D_u^{\pi^-} = D_{\bar{d}}^{\pi^-} \qquad \text{(Unfavoured FF)} \qquad (50)$$

$$D_3 = D_s^{\pi^+} = D_{\bar{s}}^{\pi^+} = D_s^{\pi^-} = D_{\bar{s}}^{\pi^-} \qquad \text{(Strange FF)}, \qquad (51)$$

reducing the number of fragmentation functions to 3. Eqn. 49 states that the probability of a u or a $\bar{d}$ quark to produce a π^+ is the same as for a d or a $\bar{u}$ quark to produce a π^-. Since these are valence quarks in the final state hadron, this

fragmentation function (D_1) is called *favoured*. The processes referred to in Eqn. 50 are more complicated and therefore D_2 should be smaller than D_1. D_2 is called the *unfavoured* fragmentation function. Plots of $D_1(z)$ and $D_2(z)$ from the HERMES [50] and EMC [51] experiments are shown in Fig. 16 where it can be seen that D_1 is several times as large as D_2 in the mid-z range. Finally D_3 is the strange fragmentation function and should be similar in size to D_2. Fragmentation (or hadronisation) is governed by long-range dynamics. It is therefore non-perturbative and we must use phenomenological models to describe it. One such simple model is the independent fragmentation model [48] which leads to:

$$\frac{D_2(z)}{D_1(z)} = \frac{1-z}{1+z}.$$
(52)

Eqn. 52 predicts $D_1{=}D_2$ at $z = 0$ where the target region dominates and the hadronisation process is complicated enough that π^-'s should be produced in the same amount as π^+'s. Eqn. 52 also predicts $D_2{=}0$ at $z = 1$. This is intuitively correct since a hadron carrying all of the energy transferred in the reaction must contain the struck quark and the unfavoured fragmentation function should therefore vanish. This behaviour is seen in Fig. 17 which is a plot of $D_2(z)/D_1(z)$ from HERMES [50] and EMC [51]. The data indicate that $D_2(z)/D_1(z)$ does not drop off with z as quickly as expected from Eqn. 52, especially for $z > 0.7$. However, the error bars are large and the high z behaviour remains to be confirmed.

9.4 Polarised Valence and Sea Quark Distributions

Valence Quarks:

The contribution to the nucleon spin from the valence quarks can be determined from the polarisation dependent yield of charged pions from two targets [45]. We will work through this example in some detail to show how an apparently complicated quantity can be written simply in terms of four quark distribution functions.

First, write out the numerator of Eqn. 48 for π^+ production on a H target when the spins of the beam and the target are opposite:

$$N_{\uparrow\downarrow}^{\pi^+} = \frac{4}{9}\, u^+ D_u^{\pi^+} + \frac{1}{9} d^+ D_d^{\pi^+} + \frac{4}{9} \bar{u}^+ D_{\bar{u}}^{\pi^+} + \frac{1}{9} \bar{d}^+ D_{\bar{d}}^{\pi^+} + \frac{1}{9} s^+ D_s^{\pi^+} + \frac{1}{9} \bar{s}^+ D_{\bar{s}}^{\pi^+}.$$
(53)

Using Eqns. 49, 50, and 51, we can re-write this as:

$$N_{\uparrow\downarrow}^{\pi^+} = \frac{4}{9} u^+ D_1 + \frac{1}{9} d^+ D_2 + \frac{4}{9} \bar{u}^+ D_2 + \frac{1}{9} \bar{d}^+ D_1 + \frac{1}{9} s^+ D_3 + \frac{1}{9} \bar{s}^+ D_3.$$
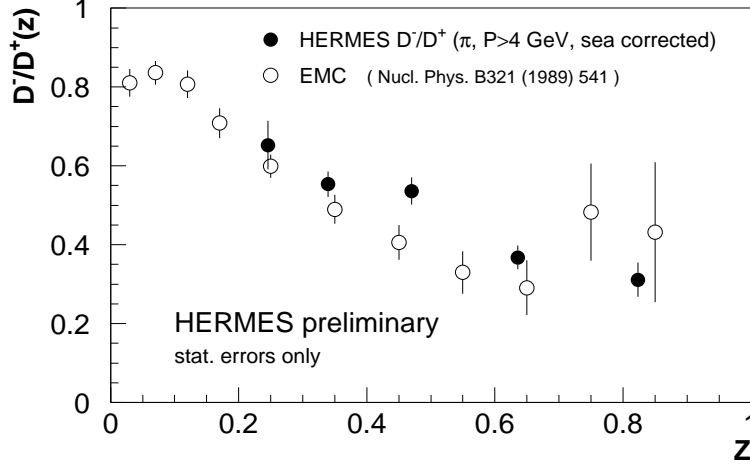(54)

33

Figure 17: Plot of the ratio of the favoured and unfavoured fragmentation functions which qualitatively shows the behaviour predicted by Eqn. 52.

A similar equation holds for the production of π^- on H with the same relative spin orientations:

$$N_{\uparrow\downarrow}^{\pi^-} = \frac{4}{9}u^+ D_2 + \frac{1}{9}d^+ D_1 + \frac{4}{9}\bar{u}^+ D_1 + \frac{1}{9}\bar{d}^+ D_2 + \frac{1}{9}s^+ D_3 + \frac{1}{9}\bar{s}^+ D_3. \qquad (55)$$

Taking the difference of Eqns. 54 and 55, the strange quark contributions drop out and the term $(D_1 - D_2)$ factors out:

$$N_{\uparrow\downarrow}^{\pi^+} - N_{\uparrow\downarrow}^{\pi^-} = \frac{4}{9}(u^+ - \bar{u}^+)(D_1 - D_2) \; - \; \frac{1}{9}(d^+ - \bar{d}^+)(D_1 - D_2). \qquad (56)$$

Since $(q^+ - \bar{q}^+)$ is just the valence distribution for quark flavour q, Eqn. 56 can finally be written as:

$$N_{\uparrow\downarrow}^{\pi^+} - N_{\uparrow\downarrow}^{\pi^-} = \frac{1}{9}(4u_v^+ - d_v^+)(D_1 - D_2). \qquad (57)$$

The sea quark contribution has been cancelled out by taking the difference of π^+ and π^- production and we are left with an expression for the valence quarks alone. A similar expression holds for the other spin direction, which is sensitive to u_v^- and d_v^-:

$$N_{\uparrow\uparrow}^{\pi^+} - N_{\uparrow\uparrow}^{\pi^-} = \frac{1}{9}(4u_v^- - d_v^-)(D_1 - D_2). \qquad (58)$$

34

Taking the difference (sum) of Eqns. 57 and 58, we get an expression which depends on the polarised (unpolarised) valence quark distribution functions:

$$(N_{\uparrow\downarrow}^{\pi^+} - N_{\uparrow\downarrow}^{\pi^-}) - (N_{\uparrow\uparrow}^{\pi^+} - N_{\uparrow\uparrow}^{\pi^-}) = \frac{1}{9}(4\Delta u_v - \Delta d_v)(D_1 - D_2), \qquad (59)$$

$$(N_{\uparrow\downarrow}^{\pi^+} - N_{\uparrow\downarrow}^{\pi^-}) + (N_{\uparrow\uparrow}^{\pi^+} - N_{\uparrow\uparrow}^{\pi^-}) = \frac{1}{9}(4u_v - d_v)(D_1 - D_2). \qquad (60)$$

Finally, the fragmentation functions cancel in the ratio of Eqns. 59 and 60 and we get:

$$\frac{(N_{\uparrow\downarrow}^{\pi^+} - N_{\uparrow\downarrow}^{\pi^-}) - (N_{\uparrow\uparrow}^{\pi^+} - N_{\uparrow\uparrow}^{\pi^-})}{(N_{\uparrow\downarrow}^{\pi^+} - N_{\uparrow\downarrow}^{\pi^-}) + (N_{\uparrow\uparrow}^{\pi^+} - N_{\uparrow\uparrow}^{\pi^-})}[\text{proton}] = \frac{4\Delta u_v - \Delta d_v}{4u_v - d_v}. \qquad (61)$$

The unpolarised quark distribution functions in the denominator have been determined from unpolarised DIS experiments so that we are left with only two unknowns in Eqn. 61. A similar expression can be written for a deuterium target:

$$\frac{(N_{\uparrow\downarrow}^{\pi^+} - N_{\uparrow\downarrow}^{\pi^-}) - (N_{\uparrow\uparrow}^{\pi^+} - N_{\uparrow\uparrow}^{\pi^-})}{(N_{\uparrow\downarrow}^{\pi^+} - N_{\uparrow\downarrow}^{\pi^-}) + (N_{\uparrow\uparrow}^{\pi^+} - N_{\uparrow\uparrow}^{\pi^-})}[\text{deuteron}] = \frac{\Delta u_v + \Delta d_v}{u_v + d_v}, \qquad (62)$$

and we can now solve for Δu_v and Δd_v separately. This is a powerful tool to isolate the contribution to the nucleon spin from the valence quarks. Note that we must be able to identify pions for this technique to work. However, the same formalism can be applied to all hadrons at the expense of extra model dependence if Monte Carlo techniques are used to calculate corrections for the fact that the type of final state hadron is not determined. Note also that data on *two* targets are needed to determine the polarised valence quark distributions using this technique.

Sea Quarks:

Different combinations of identified hadron yields can be used to isolate different quark distributions. In particular since π^- is a $\bar{u}d$ state and that the coupling in DIS scattering is four times larger for the $\bar{u}$ quark than for the d quark, polarisation dependent π^- production should be sensitive to the polarised $\bar{u}$ distribution. Furthermore, since K^- is a $\bar{u}s$ state, it is *all sea* and should have increased sensitivity, especially to the strange sea[46]. Expressions for π^- and K^- production based on Eqn. 48 can be derived in a similar way to the previous section.
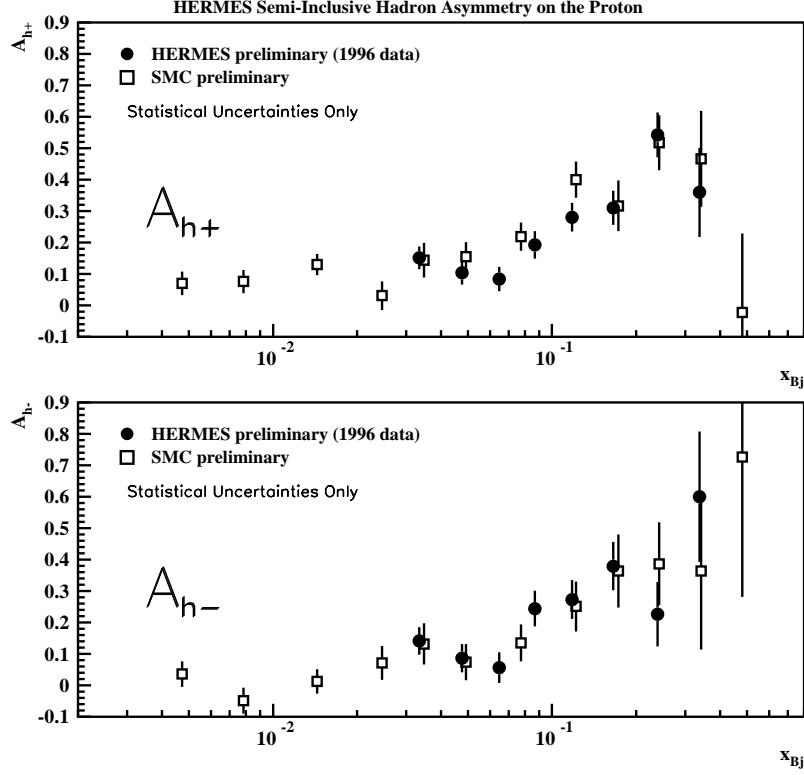
Figure 18: Single hadron asymmetries from SMC[52] and HERMES[53] for a H target.

Once high-statistics data sets exist on the production of $\pi^\pm$ and $K^\pm$ on more than one target, a global fitting procedure can be used to determine all polarised quark distributions at once (see next section). It is hoped that such data sets will be available in the next two years.

9.5 Single Hadron Asymmetries and Polarised Quark Distributions

Single Hadron Asymmetries

Semi-inclusive data are usually presented in the form of single hadron asymmetries defined as follows:

$$A_h = \frac{N_{\uparrow\downarrow}^h - N_{\uparrow\uparrow}^h}{N_{\uparrow\downarrow}^h + N_{\uparrow\uparrow}^h}. \tag{63}$$
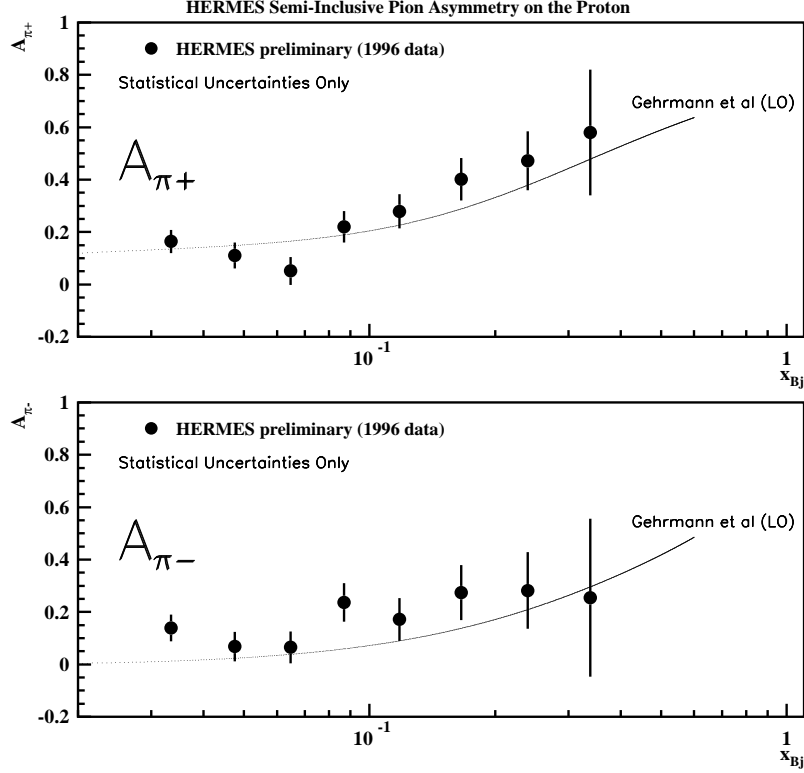
Figure 19: Single pion asymmetries from HERMES[53] for a H target. The data are compared to quark distributions from a leading order fit by Gehrmann and Stirling[30].

Data on semi-inclusive processes exist only from HERMES and SMC, with identified pions only available at HERMES. The acceptance of the SLAC spectrometers makes detection of a hadron in coincidence essentially impossible. SMC has data for both H and D, while HERMES currently only has data on H and ^{3}He (D will be run in 1998-99). The charged hadron single spin asymmetries for the proton are shown in Fig. 18 for SMC[52] and HERMES[53]. The error bars are comparable. However only one third of the HERMES data are included in this plot. As in the inclusive case, the SMC data go to lower x because of the higher beam energy. The data quality is already quite good and will be improved when HERMES finishes the analysis of the 1997 data. The asymmetries are positive and rather large, especially at $x \geq 0.1$.

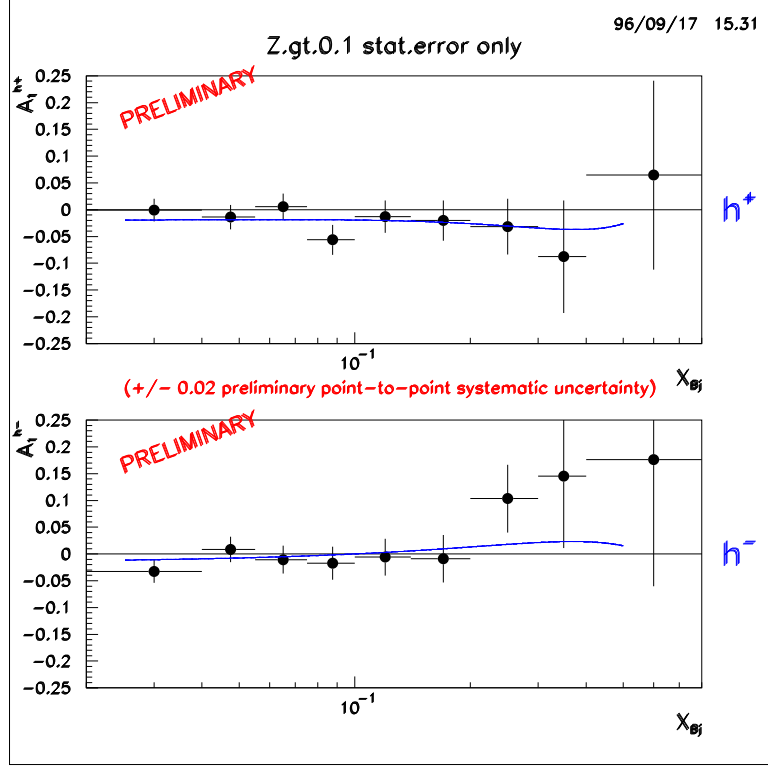Pion asymmetries from HERMES[53] are shown in Fig. 19 where they are

Figure 20: Single hadron asymmetries from HERMES[54] for a ^{3}He target.

compared to the fit of quark distribution functions by Gehrmann and Stirling[30]. Note that here too, only one third of the data have been analysed.

Finally, Fig. 20 shows the hadron asymmetries measured by HERMES[54] on a ^{3}He target in 1995. Since this was the commissioning year for the experiment, the statistics are quite low and the error bars are correspondingly large. However, it is clear that the asymmetries are much smaller for the neutron than for the proton as in the inclusive case. The data set for the neutron will be improved significantly in 1998-99 when HERMES runs with a deuterium target.

Polarised Quark Distributions; the Purity Method

The best way to determine the polarised quark distribution functions has been to perform a global fit to the inclusive data. The same can be done includ-

ing the semi-inclusive data when a sufficiently large data base has been accumulated. We can write the single hadron asymmetries in terms of quark distribution functions and fragmentation functions:

$$A_1^h = \frac{1}{D} \frac{N_{\uparrow\downarrow}^h - N_{\uparrow\uparrow}^h}{N_{\uparrow\downarrow}^h + N_{\uparrow\uparrow}^h} = \frac{\sum_i e_i^2 \; \Delta q_i(x,Q^2) \; D_i^h(z,Q^2)}{\sum_i e_i^2 \; q_i(x,Q^2) \; D_i^h(z,Q^2)} \; (1 + R(x,Q^2)), \quad (64)$$

where the sum is over quarks and anti-quarks separately and $R = \sigma_L/\sigma_T$ as seen earlier. The $(1+R)$ term is needed to be consistent with the extraction of the unpolarised quark distribution functions using F_2 which does not assume $R = 0$. We can define functions P_i^h, called *Purities*, as the probability that a hadron h was produced by the fragmentation of a quark q_i that was struck in the DIS process [55]. These are similar to the fragmentation functions but should not be confused with them. The purities are written as follows:

$$P_i^h(x,Q^2,z) = \frac{e_i^2 \; q_i(x,Q^2) \; \int_{0.2}^1 D_i^h(z)\,dz}{\sum_j e_j^2 \; q_j(x,Q^2) \; \int_{0.2}^1 D_j^h(z)\,dz}. \quad (65)$$

We can now re-write Eqn. 64 in terms of purities and quark polarisations:

$$A_1^h(x) = \sum_q P_q^h(x) \; \frac{\Delta q(x)}{q(x)} \; (1 + R(x)). \quad (66)$$

The purities can be calculated by Monte Carlo and hence can also contain information about the acceptance of the spectrometer and detector effects. Purities can also be defined for inclusive asymmetries as follows:

$$P_q^e(x,Q^2) = \frac{e_q^2 \; q(x,Q^2)}{\sum_q e_q^2 \; q(x,Q^2)}, \quad (67)$$

and give the probability that the inclusive scattering came from quark q. If one combines inclusive and semi-inclusive measurements, Eqn. 66 becomes a matrix equation and we can determine the polarised quark distribution functions by inverting the purity matrix. For example, consider the asymmetries for inclusive positrons ($A_1^{e^+}$), and charged pion production ($A_1^{\pi^+}$ and $A_1^{\pi^-}$):

$$\begin{pmatrix} A_1^{e^+} \\ A_1^{\pi^+} \\ A_1^{\pi^-} \end{pmatrix} = \begin{pmatrix} P_u^e & P_d^e & P_{\bar{q}}^e \\ P_u^{\pi^+} & P_d^{\pi^+} & P_{\bar{q}}^{\pi^+} \\ P_u^{\pi^-} & P_d^{\pi^-} & P_{\bar{q}}^{\pi^-} \end{pmatrix} \begin{pmatrix} \Delta u/u \\ \Delta d/d \\ \Delta \bar{q}/\bar{q} \end{pmatrix}. \quad (68)$$

The $(1+R)$ term is now included in the matrix P. More data can be included to get a larger matrix equation and determine more quark distribution functions.
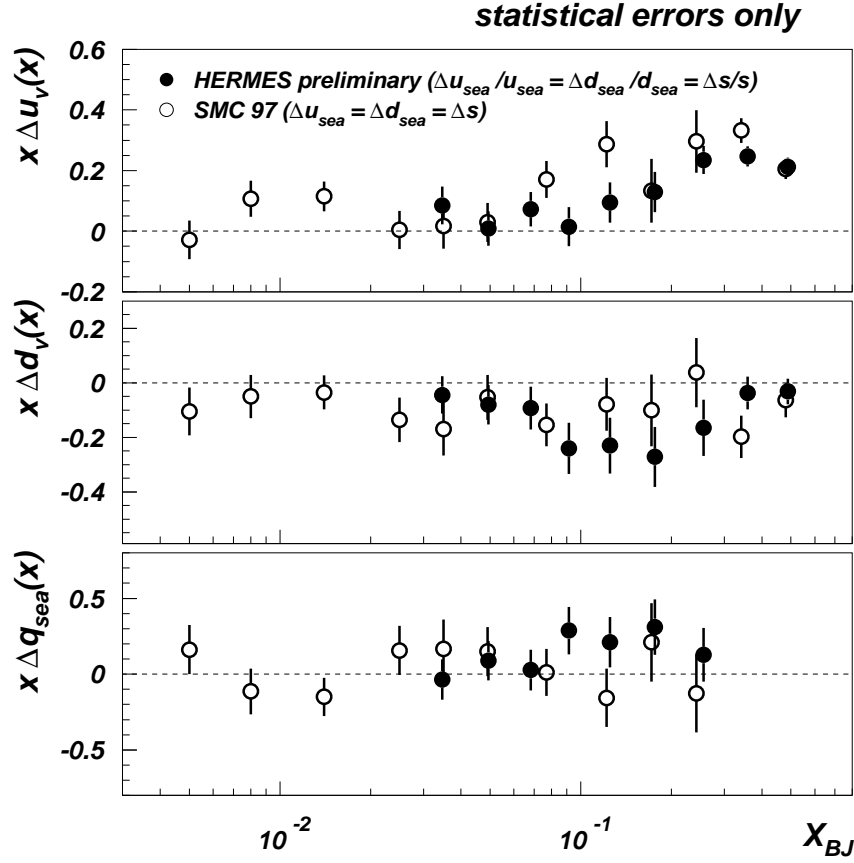
39

statistical errors only

Figure 21: Polarised quark distributions from a fit to SMC data [52] and using the purity method for HERMES 1996 data [55]. Distributions are plotted for valence u and d quarks as well as for the sea $\bar{q}$ under the assumption that the polarisation of the u_{sea}, d_{sea}, and s quarks is the same.

40

Care must be taken when inverting the purity matrix because the data are correlated (e.g. the semi-inclusive data are a sub-set of the inclusive data) and the uncertainties must be calculated correctly. For more details, see the contribution to this workshop by M.-A. Funk.

Results from SMC[52] and HERMES (1996 only)[55] are shown in Fig. 21 for the polarised valence quark distributions as well as for the sea distribution $\bar{q}$. It is not possible with the current data to separate the contribution from each type of sea quark. New data to be taken in the next two years at HERMES with the RICH detector and with two targets (D and H) will greatly improve the situation.

9.6 Charm Production and the Gluon Contribution

While data collected to date on inclusive and semi-inclusive polarised DIS are sensitive to the spins of the quarks, we saw earlier that it is now crucial to determine if the gluons are polarised. In order to be sensitive to gluon polarisation, the normal DIS diagrams must be suppressed. One way to do this is by considering charm production. This has proven to be useful in the unpolarised case [56]. There should not be a large charm component in the nucleon wavefunction (intrinsic charm) so it is not very probable to strike a charm quark directly. Furthermore, charm production in the fragmentation of light quarks is suppressed by the mass of the charm quark. As a result, charm production in DIS is dominated by photon-gluon fusion which is shown diagrammatically in Fig. 22. In this process, the virtual photon and the gluon interact through the intermediary of a $c\bar{c}$ pair. The charm quarks can manifest themselves as charmed mesons in the final state (open charm production: D-mesons), or as J/ψ mesons (hidden charm). In the latter case, a second gluon must be emitted by the $c\bar{c}$ system in order to get a colour singlet final state. If this gluon is soft, the interpretation of the process becomes more difficult. Therefore, conditions must be placed on the kinematics of the reaction to ensure that we have inelastic J/ψ's in the final state. The asymmetry in charm production for the two relative spin states of the beam and the target can be written as:

$$A_{LL}(z, p_T) = \hat{a}_{LL} \frac{\Delta g}{g} \tag{69}$$

where p_T is the transverse momentum of the charm meson, and $\hat{a}_{LL}$ is the asymmetry for the elementary hard scattering process (i.e. $\gamma - c$). The asymmetry depends on the production mechanism. It has been calculated for J/ψ production in the colour singlet model [57] by Guillet [58] and is ≈ 0.5 for HERMES kinematics. $\hat{a}_{LL}$ has also been estimated in the colour octet model which
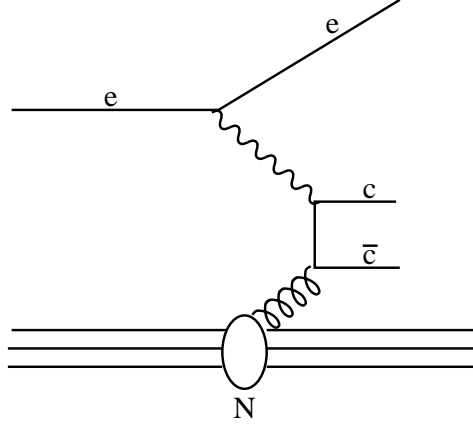
41

Figure 22: Diagram of the photon-gluon fusion process. The photon and the gluon couple through the intermediary of a $c\bar{c}$-pair.
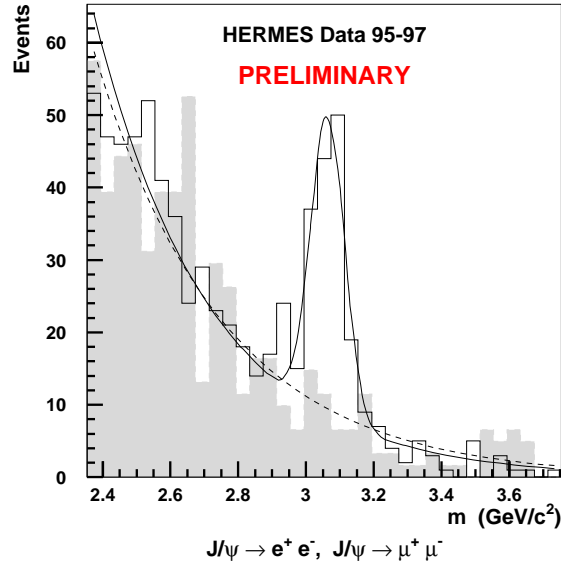

Figure 23: J/ψ mass peak in the e$^+$-e$^-$ and μ^+-μ^- decay channels at HERMES. The efficiency for μ identification will be significantly improved for 1998.

42

might be more applicable at high z. In this case $\hat{a}_{LL}$=1 so that the asymmetry is likely to be large in either model. J/ψ's have been clearly identified at HER-MES (Fig. 23) and the projected accuracy on $\Delta g/g$ is 0.52 after the '98-'99 running period and 0.38 by 2001 [59]. This will be reduced if improvements to the target can be made. While this accuracy is limited, HERMES should be able to make a qualitative statement on whether Δg is non-zero.

An advantage of open-charm production is the larger cross-section compared to J/ψ production. This is particularly important at HERMES where the c.m. energy is barely above threshold. On the other hand, the identification of D-mesons is more difficult than J/ψ, especially without K/π separation in the hadron PID.

10 The Future of the Field

HERMES is the only running polarised DIS experiment for the moment. SLAC has approved an extension to E155 to collect high statistics data with a transversely polarised target to improve the data on g_2. This experiment should run in 1999. An experiment called COMPASS is being prepared at CERN to measure semi-inclusive DIS, in particular open charm production at higher beam energy than HERMES to study the gluon polarisation. The capability to have polarised protons in RHIC is being included in the accelerator design. The physics to be addressed in high energy $\vec{p}$-$\vec{p}$ collisions is described briefly below and in another contribution to these proceedings [64]. Finally, DESY is studying the possibility to accelerate polarised protons in HERA to study polarised DIS at very small values of x.

10.1 HERMES Upgrades

HERMES has embarked on an upgrade program for the 1998 run and beyond to include kaon identification and improve the efficiency for the detection of charm mesons [59,60,61]. A schematic of the HERMES upgrades is shown in Fig. 24.

Hadron identification will be greatly improved by replacing the threshold Čerenkov detector by a Ring Imaging Čerenkov detector (RICH) [60]. The RICH will use a dual radiator system: C_4F_{10} gas with an index of refraction of 1.0014 and clear aerogel with n=1.03. The Čerenkov photons will be detected by an array of 3/4" phototubes (roughly 2000 per half). The RICH will provide identification of pions, kaons, and protons (and p̄) over most of the kinematic range of the experiment (2-20 GeV). This will allow HERMES to measure all hadron asymmetries and thus determine the contribution of each quark species
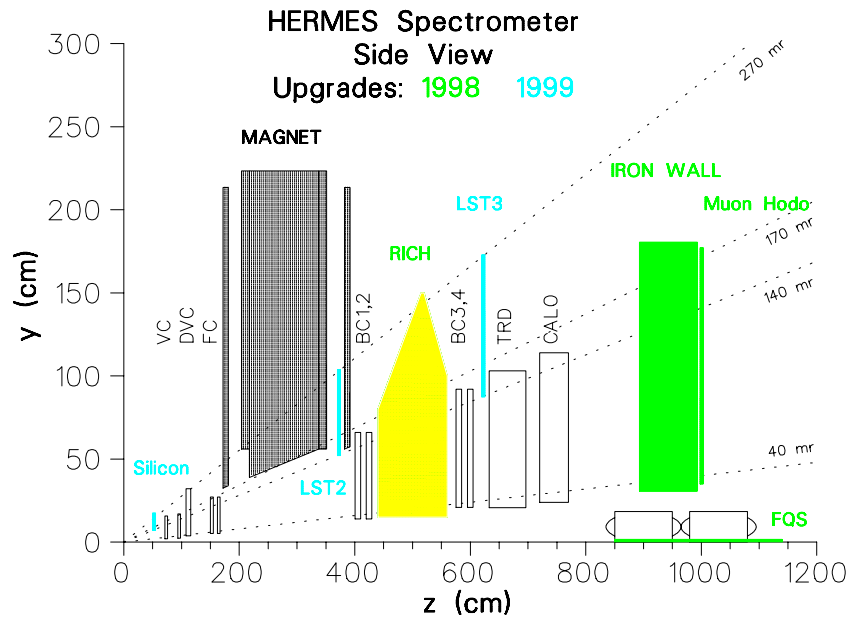
43

Figure 24: Schematic representation of the upgrades to the HERMES spectrometer. The RICH, the iron wall for muon identification, and the FQS to measure the kinematics of electrons from low Q^2 events will all be ready for the 1998 running period. The limited streamer tubes to increase the acceptance for μ^+-μ^- pairs and most of the silicon-strip detectors in the target chamber will not be ready until 1999.

to the nucleon's spin. Furthermore, kaon identification will allow the detection of D-mesons through the K-π decay channel.

Further improvements to the charm detection efficiency will be made on three fronts[59]. First, an iron wall to absorb hadrons has been erected behind the calorimeter followed by a scintillator hodoscope. This system will improve the muon identification and double the number of J/ψ particles detected by including the $\mu^+\mu^-$ decay channel. Better muon identification will also help for semi-leptonic D-meson decays. The second upgrade related to charm is a Forward Quadrupole Spectrometer (FQS) which will be installed in the first two machine quadrupoles downstream of the experiment. This device will detect electrons from low-Q^2 events, which are scattered down the beampipe. This will allow full kinematic reconstruction of these events and help separate elastic (or diffractive) J/ψ production from events which can be interpreted in terms of Δg. Finally, the acceptance for J/$\psi \rightarrow \mu^+\mu^-$ will be increased by extending the tracking in front of the magnet and instrumenting the corresponding region behind the magnet steel which will act as a muon filter. The enlarged $\mu^+\mu^-$ acceptance will greatly increase the J/ψ sample since most of these particles are produced with very low energy and hence with a large opening angle for the decay muons.

HERMES is also preparing two arrays of silicon-strip detectors to be located inside the target chamber[61]: two wheel-shaped detectors between the storage cell and the exit window (Λ-wheels), and recoil detectors parallel to the storage cell. The recoil detector has many functions. It can detect slow recoil protons in e-d scattering to tag e-n events and eliminate nuclear corrections. The detection of a recoil proton in J/ψ-production can be used to eliminate elastic events and also to help reconstruct decays where only one of the leptons is in the spectrometer acceptance. As their name implies, the Λ wheels will be used to study Λ production and the subsequent decay to $p + \pi^-$ (Λ) or $\bar{p} + \pi^+$ ($\bar{\Lambda}$). The idea is to take advantage of the fact that the Λ-decay is self-analysing making it possible to measure the polarisation of the Λ's. This polarisation can be written as:

$$P_\Lambda = (P_B D + P_T \frac{\Delta u}{u}) \ \frac{\Delta u^\Lambda}{u^\Lambda} \tag{70}$$

where P_B and P_T are the beam and target polarisations respectively, D is a depolarisation factor and $\Delta u/u$ and $\Delta u^\Lambda/u^\Lambda$ are the polarisations of the u-quark in the proton and the Λ. With an unpolarised target, $\Delta u^\Lambda/u^\Lambda$ can be determined and the spin transfer from the u-quark in the proton to the Λ can be measured. If we assume that this quantity does not depend on the target orientation, we can then determine the transverse polarisation of u-quarks

in the proton by measuring P_Λ with a transversely polarised target. While the current acceptance of the HERMES spectrometer is not well matched to Λ detection, the Λ-wheels will substantially increase the acceptance and also extend the range for negative values of x_F.

10.2   COMPASS at CERN

The COMPASS experiment at CERN is being designed to study semi-inclusive processes at a higher energy than HERMES (100 GeV muons) [62]. The goal is to measure $\Delta g/g$ to an accuracy of 0.11 after 1.5 years of data taking. The main advantage over HERMES is the much higher charm production cross-section due to the higher beam energy. The principal channels to be studied are:

$$D^0 \to K^- \pi^+ \;\; ; \;\; \bar{D}^0 \to K^+ \pi^-.$$

A two stage spectrometer with very large acceptance is being built. Good hadron identification will be provided by two RICH detectors. The targets will be similar to those used at SMC and E155: NH_3 (85% polarisation) and LiD (50% polarisation). COMPASS will also make the semi-inclusive measurements described in Sec. 9. The experiment is expected to start data taking in 2000.

10.3   Polarised beams at RHIC

The capability to study collisions of 250 GeV polarised protons at RHIC is being prepared [63]. A more complete description of this program is given in the contribution to these proceedings by J. Harris [64] and the reader is referred to this paper. Briefly, the polarisation of the sea quarks can be measured using the Drell-Yan process ($q\bar{q} \to \mu^+ \mu^-$), while sensitivity to the gluon polarisation can be obtained by studying the production of isolated photons (the so-called direct photon process: $qg \to \gamma q$), jet production, or J/ψ production. The direct photon experiment is challenging because of the large background of γ's from π^0 decays. While it is possible to isolate gg-processes by using the characteristics of jets (e.g. the invariant mass of the 2-jet system), the interpretation is more difficult than for the direct photon process. RHIC is scheduled to produce heavy ion collisions in 1999 and it is expected that some time could be set aside for polarised protons as early as 2000.

10.4   Polarised Protons at HERA

In the long term ($\approx$2005), DESY is studying the possibility of accelerating polarised protons in HERA [65,66] which would allow the extension of the data set on g_1 down to very low x. One of the problems associated with this program

is the small depolarisation factor D due to the kinematics of the scattering. This means that the polarisation of the virtual photons is small and very high luminosity is required to compensate. Furthermore, getting polarised protons through the accelerator chain at DESY is not trivial and will involve the use of partial Siberian snakes in PETRA and as many as four full snakes in HERA. Nevertheless, information on g_1 at low x is crucial to our understanding of how to do the extrapolation to $x = 0$. HERA would extend the minimum x from about 5.10^{-3} down to a few times 10^{-5}. Furthermore, asymmetries in the production of jets are expected to be large and will give information on Δg.

10.5 Real photon experiments

Finally, experiments on charm production using real photons have been proposed both at SLAC (E156) and at DESY (APOLLON). However, neither of these has been approved and they are on hold until further notice.

11 Summary

A pedagogical overview of the field of nucleon spin physics has been presented in these lectures. Ongoing technological advances in polarised target and beam production have made possible a series of experiments over the last 10 years to study how the spin of the nucleon is related to the spins of its constituents. There now exists a large body of data on inclusive polarised deep inelastic scattering from CERN, SLAC, and DESY. These data indicate that only a small fraction of the nucleon's spin comes from the spins of the quarks. While the Bjorken sum rule has been verified to about 10% accuracy, the data on the integrals of $g_1(x)$ for the proton and the neutron disagree with the predictions of the Ellis-Jaffe sum rules by one to several sigma. Further progress in this field will be based on semi-inclusive measurements where the flavour of the struck quark can be tagged by the type of hadron produced in the final state. This will allow the contributions from valence and sea quarks to be isolated. The production of charmed mesons will give information on the polarisation of the gluons. The HERMES experiment which will run with a deuterium target in 1998-99 will produce complete data sets on semi-inclusive pion and kaon production for the proton and the neutron. HERMES will also study charm production and should be able to make a qualitative statement on whether the gluons are polarised. A precise determination of Δg must await the new experiments being planned at CERN (COMPASS) and at Brookhaven (Spin-RHIC). The next few years promise to be very exciting in this field and we

might finally find a solution to the "nucleon spin puzzle".

Acknowledgments

References

1. *"Deep Inelastic Scattering and Related Phenomena"*, Proceedings of the DIS96 conference, Rome, Italy, April 1996, editors: G. D'Agostini and A. Nigro. World Scientific, ISBN# 981-02-3008-7.
2. *"Deep Inelastic Scattering and QCD"*, Proceedings of the DIS97 conference, Chicago, Illinois, April 1997, editors: J. Repond and D. Krakauer. AIP Conference Proceedings, ISBN# 1-56396-716-2.
3. D.H. Perkins, *"Introduction to High Energy Physics"*, 3rd edition, Addison-Wesley, ISBN# 0-201-12105-0.
4. F. Halzen and A.D. Martin, *"Quarks and Leptons: An Introductory Course in Modern Particle Physics"*, Wiley, ISBN# 0-471-88741-2.
5. F.E. Close, *"An Introduction to Quarks and Partons"*, Academic Press, ISBN# 0-12-175152-x.
6. D. Griffiths, *"Introduction to Particle Physics"*, Wiley, ISBN# 0-471-60386-4.
7. R.G. Roberts, *"The Structure of the Proton"*, Cambridge Monographs on Mathematical Physics, ISBN# 0-521-35159-6.
8. C.G. Callan and D. Gross, *Phys. Rev. Lett.* **22**, 156 (1969).
9. L.W. Whitlow *et al.*, *Phys. Lett.* B **250**, 193 (1990).
10. J. Ashman *et al.*, *Phys. Lett.* B **206**, 364 (1988).
11. D. Adams *et al.*, *Phys. Rev.* D **56**, 5330 (1997).
12. D. Adams *et al.*, *Phys. Lett.* B **396**, 338 (1997).
13. P.L. Anthony *et al.*, *Phys. Rev.* D **54**, 6620 (1996).
14. K. Abe *et al.*, *Phys. Rev. Lett.* **74**, 346 (1995).
15. K. Abe *et al.*, *Phys. Rev. Lett.* **75**, 25 (1995).
16. The HERMES Collaboration, preliminary. Final results submitted to *Phys. Lett.* B; DESY preprint 98-072; hep-ex/9807015.

17. K. Ackerstaff *et al.*, *Phys. Lett.* B **404**, 383 (1997).

18. K. Abe *et al.*, *Phys. Rev. Lett.* **79**, 26 (1997).

19. J.D. Bjorken, *Phys. Rev.* **148**, 1467 (1966) and *Phys. Rev.* D **1**, 1376 (1970).

20. S.A. Larin, F.V. Tkachev, and J.A.M. Vermaseren, *Phys. Rev. Lett.* **66**, 862 (1991); and S.A. Larin and J.A.M. Vermaseren, *Phys. Lett.* B **259**, 345 (1991).

21. J. Ellis and R.L. Jaffe, *Phys. Rev.* D **9**, 1444 (1974) and *Phys. Rev.* D **10**, 1669 (1974).

22. F.E. Close and R.G. Roberts, *Phys. Lett.* B **316**, 165 (1993).

23. K. Abe *et al.*, *Phys. Lett.* B **405**, 180 (1997).

24. G. Altarelli, R.D. Ball, S. Forte, and G. Ridolfi, *Nucl. Phys.* B **496**, 337 (1997).

25. G. Altarelli and G. Parisi, *Nucl. Phys.* B **126**, 298 (1977).

26. G. Altarelli and G.G. Ross, *Phys. Lett.* B **212**, 391 (1988).

27. K. Abe *et al.*, *Phys. Lett.* B **364**, 61 (1995).

28. M. Glück, E. Reya, M. Stratmann, ans W. Vogelsang, *Phys. Rev.* D **53**, 4775 (1996).

29. R.D. Ball, S. Forte, and G. Ridolfi, *Nucl. Phys.* B **444**, 287 (1995); erratum *Nucl. Phys.* B **449**, 680 (1995).

30. T. Gehrmann and W.J. Stirling, *Phys. Rev.* D **53**, 6100 (1996).

31. R.L. Jaffe and X. Ji, *Phys. Rev.* D **43**, 724 (1991).

32. A.V. Manohar, *"Symmetry and Spin in the Standard Model"*, Proceedings of the 7th Lake Louise Winter Institute, February 1992, editors: B.A. Campbell, L.G. Greenius, A.N. Kamal, and F.C. Khanna, World Scientific, ISBN# 981-02-1034-5.

33. W. Wandzura and F. Wilczek, *Phys. Lett.* B **72**, 195 (1977).

34. K. Abe *et al.*, *Phys. Rev. Lett.* **76**, 587 (1996).

35. M. Stratmann, *Z. Phys.* C **60**, 763 (1993).

36. X. Song and J.S. McCarthy, *Phys. Rev.* D **49**, 3169 (1994).

37. H. Burkhardt and W.N. Cottingham, *Ann. Physics* **56**, 453 (1970).

38. R.L. Jaffe and X. Ji, *Phys. Rev. Lett.* **67**, 552 (1991).

39. P. Hoodbhoy, R.L. Jaffe, and A. Manohar, *Nucl. Phys.* B **312**, 571 (1989); and R.L. Jaffe and A. Manohar, *Nucl. Phys.* B **321**, 343 (1989).

40. R.L. Jaffe and A. Manohar, *Phys. Lett.* B **223**, 218 (1989).

41. A.A. Sokolov and I.M. Ternov, *Sov. Phys. Doklady* **8**, 1203 (1964).

42. D.P. Barber *et al.*, *Nucl. Instrum. Methods* A **329**, 79 (1993); and D.P. Barber *et al*, *Phys. Lett.* B **343**, 436 (1995).

43. D. De Schepper *et al.*, Submitted to *Nucl. Instrum. Methods*; and Ph.D. thesis, Massachusetts Institute of Technology, Boston, MA, June 1991;

HERMES internal note #97-022*.

44. K. Ackerstaff *et al.*, Accepted in *Nucl. Instrum. Methods*, DESY preprint #98-057; hep-ex/9806008.

45. L.L. Frankfurt *et al.*, *Phys. Lett.* B **230**, 141 (1989).

46. F.E. Close and R.G. Milner, *Phys. Rev.* D **44**, 3691 (1991).

47. E.L. Berger, *"Semi-Inclusive Inelastic Electron Scattering from Nuclei"*, Proceedings of the Workshop on Electronuclear Physics with Internal Targets, Stanford, CA, January 1987; ANL-HEP-PR-87-45.

48. R.D. Field and R.P. Feynman, *Phys. Rev.* D **15**, 2590 (1977) and *Nucl. Phys.* B **136**, 1 (1978)

49. J. Binnewies, B.A. Kniehl, and G. Kramer, *Phys. Rev.* D **52**, 4947 (1995).

50. P. Geiger, *"Measurement of Fragmentation Functions at HERMES"*, Ph.D. thesis, Ruprecht Karl Universität, Heidelberg, Germany, February 1998; HERMES internal note #98-005*.

51. M. Arneodo *et al.*, *Nucl. Phys.* B **321**, 541 (1989).

52. B. Adeva *et al.*, *Phys. Lett.* B **420**, 180 (1998).

53. F.M. Menden, *"Measurement of the Valence Quark Spin Distributions of the Nucleon Using Deep Inelastic Scattering at HERMES"*, Diploma thesis, Universität Hamburg and TRIUMF, October 1997; HERMES internal note #98-001*.

54. K.P. Schüler, *"HERMES Semi-Inclusive Results"*, Proceedings of the DIS98 conference, Chicago, Il, April 1997, editors: J. Repond and D. Krakauer. AIP Conference Proceedings, ISBN# 1-56396-716-2.

55. M.A. Funk, *"A Measurement of the Polarised Parton Densities of the Nucleon in Deep Inelastic Scattering at HERMES"*, Ph.D. thesis, Universität Hamburg, June 1998; HERMES internal note #98-034*; and Contribution to these proceedings.

56. D. Allasia *et al.*, *Phys. Lett.* B **258**, 493 (1991).

57. E.L. Berger and D. Jones, *Phys. Rev.* D **23**, 1521 (1981).

58. J.Ph. Guillet, *Z. Phys.* C **39**, 75 (1988).

59. M. Amarian *et al.*, *"The HERMES Charm Upgrade Program"*, Proposal to the DESY-HERA PRC, January 1997; HERMES internal note #97-004*.

60. E. Cisbani *et al.*, *"Proposal for a Dual Radiator RICH for HERMES"*, Proposal to the DESY-HERA PRC, January 1997; HERMES internal note #97-003*.

61. The HERMES Collaboration, *"New Silicon Detector Systems for the HERMES Front Region"*, Proposal to the DESY-HERA PRC, October 1997; HERMES internal note #97-032*.

62. The COMPASS Collaboration *"Common Muon and Proton Apparatus for Structure and Spectroscopy"*, CERN/SPSLC 96-14, March 1996.
63. *"Proposal on Spin Physics using the RHIC Polarized Collider"*, AGS/RHIC Proposal, August 1992; update September 1993.
64. J. Harris, Contribution to these proceedings.
65. *"Deep Inelastic Scattering off Polarized Targets: Theory Meets Experiment"*, Proceedings of the workshop, Zeuthen, September 1997, editors: J. Blümlein, A. De Roeck, T.Gehrmann, and W.D. Nowak, DESY 97-200.
66. *"Future Physics at HERA"*, Proceedings of the workshop, 1995-96, editors: G. Ingelmann, A. De Roeck, and R. Klanner, DESY 95-200.

* The HERMES internal notes mentioned in the references can be obtained from the HERMES web pages: `http://www-hermes.desy.de/notes/`.